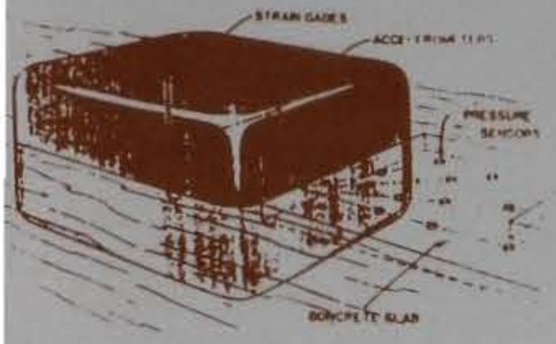


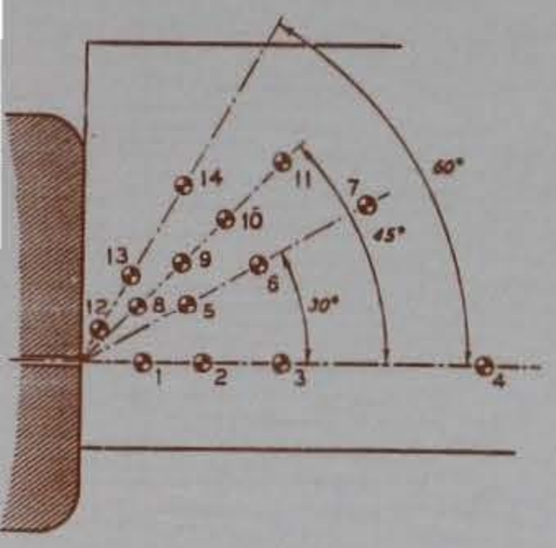


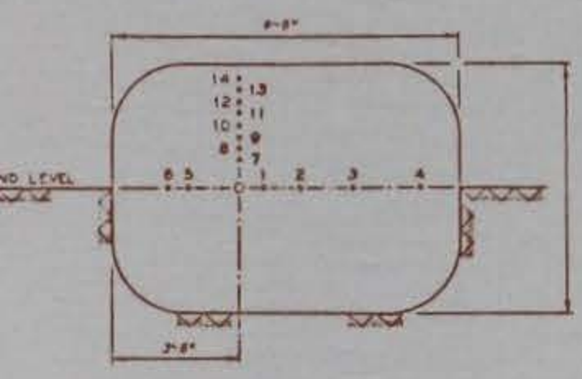






TECHNICAL REPORT SL-89-15

# EFFECTS OF EXPLOSIONS IN UNDERGROUND MAGAZINES

by

Dennis R. Smith, Charles E. Joachim, Landon K. Davis
Gordon W. McMahon

Structures Laboratory

DEPARTMENT OF THE ARMY
Waterways Experiment Station, Corps of Engineers
3909 Halls Ferry Road, Vicksburg, Mississippi 39180-6199

October 1989
Final Report

Approved For Public Release; Distribution Unlimited



Prepared for Department of Defense Explosive Safety Board
Alexandria, Virginia 22333

Unclassified
SECURITY CLASSIFICATION OF THIS PAGE

# REPORT DOCUMENTATION PAGE

Form Approved
OMB No. 0704-0188

1a. REPORT SECURITY CLASSIFICATION
Unclassified

1b. RESTRICTIVE MARKINGS

2a. SECURITY CLASSIFICATION AUTHORITY

2b. DECLASSIFICATION/DOWNGRADING SCHEDULE

3. DISTRIBUTION/AVAILABILITY OF REPORT
Approved for public release; distribution unlimited.

4. PERFORMING ORGANIZATION REPORT NUMBER(S)
Technical Report SL-89-15

5. MONITORING ORGANIZATION REPORT NUMBER(S)

6a. NAME OF PERFORMING ORGANIZATION
USAEWES
Structures Laboratory

6b. OFFICE SYMBOL (*If applicable*)
CEWESSE-R

7a. NAME OF MONITORING ORGANIZATION

6c. ADDRESS (*City, State, and ZIP Code*)
3909 Halls Ferry Road
Vicksburg, MS 39180-6199

7b. ADDRESS (*City, State, and ZIP Code*)

8a. NAME OF FUNDING/SPONSORING ORGANIZATION
Department of Defense Explosive Safety Board

8b. OFFICE SYMBOL (*If applicable*)

9. PROCUREMENT INSTRUMENT IDENTIFICATION NUMBER

8c. ADDRESS (*City, State, and ZIP Code*)
Alexandria, VA 22333

10. SOURCE OF FUNDING NUMBERS

| PROGRAM ELEMENT NO. | PROJECT NO. | TASK NO. | WORK UNIT ACCESSION NO. |
|---|---|---|---|
| | | | |

11. TITLE (*Include Security Classification*)
Effects of Explosions in Underground Magazines

12. PERSONAL AUTHOR(S)
Smith, Dennis R.; Joachim, Charles E.; Davis, Landon K.; and McMahon, Gordon W.

| 13a. TYPE OF REPORT | 13b. TIME COVERED | 14. DATE OF REPORT (*Year, Month, Day*) | 15. PAGE COUNT |
|---|---|---|---|
| Final Report | FROM _____ TO _____ | October 1989 | 93 |

16. SUPPLEMENTARY NOTATION
Available from National Technical Information Service, 5285 Port Royal Road, Springfield, VA 22161.

| 17. COSATI CODES | | |
|---|---|---|
| FIELD | GROUP | SUB-GROUP |
| | | |
| | | |

18. SUBJECT TERMS (*Continue on reverse if necessary and identify by block number*)
Ammunition
Explosives safety
Explosives storage
Underground storage

19. ABSTRACT (*Continue on reverse if necessary and identify by block number*)

Equations were developed to predict the safe standoff distances from accidental explosions in magazines sited in rock. The ground shock threat to adjacent chambers is considered as well as the airblast which vents through the portal. The equations relate free-field motion to geometrical effects (for cylindrical chambers), explosive coupling properties of the medium, and type and quality of explosives. A dimensionless equation was developed which delineates the upper bound of external airblast pressure as a function of the exit pressure, access tunnel diameter and distance. The experimental program was conducted with a 1:75-scale model of an underground magazine which was loaded with various explosive quantities. Measurements included airblast pressure/time outside the model, strain and particle acceleration at different distances from the magazine in the simulated rock (a cement grout). Estimated particle velocities at adjacent chambers were derived from the free-field acceleration and strain data. A spall criterion was used to estimate safe separation distances to prevent sympathetic detonation in adjacent chambers. Details of the tests and data are presented.

20. DISTRIBUTION/AVAILABILITY OF ABSTRACT
☒ UNCLASSIFIED/UNLIMITED ☐ SAME AS RPT. ☐ DTIC USERS

21. ABSTRACT SECURITY CLASSIFICATION
Unclassified

22a. NAME OF RESPONSIBLE INDIVIDUAL

22b. TELEPHONE (*Include Area Code*)

22c. OFFICE SYMBOL

DD Form 1473, JUN 86 *Previous editions are obsolete.*

SECURITY CLASSIFICATION OF THIS PAGE
Unclassified

## PREFACE

This study was conducted in 1979-80 by the Explosion Effects Division (EED), Structures Laboratory (SL), of the US Army Engineer Waterways Experiment Station (WES) for the Department of Defense Explosive Safety Board (DDESB). Dr. T. Zaker guided and monitored the study for DDESB.

The study was conceived jointly by Mr. L. F. Ingram, Mr. J. L. Drake, and Dr. Dennis R. Smith of the EED. Mr. Ingram provided overall supervision, Mr. Drake provided technical consultation and managerial functions, and Dr. Smith served as principal investigator and initial author of this report. Mr. C. E. Joachim, Mr. G. W. McMahon, and Mr. L. K. Davis completed the report in 1989.

The experimental work was performed by Messrs. S. E. Bartlett, W. Washington, and J. H. Stout. Mr. D. P. Biggs of the Instrumentation Services Division recorded the instrumentation. Mr. J. T. Brogan and Mrs. D. W. McAlpin, EED, performed the data processing. Typing of the draft report was done by Mses. Sharon McDonald, ISD, and Modell Stephenson, Lynnette Smith and Donna Richey, EED.

During the completion and publication of this report, Mr. L. K. Davis was Chief, EED, and Mr. Bryant Mather was Chief, SL. COL Larry B. Fulton, EN, was the Commander and Director of WES, and Dr. Robert W. Whalin was Technical Director.

CONTENTS

CONTENTS

## LIST OF TABLES

## LIST OF FIGURES

## LIST OF FIGURES

## CONVERSION FACTORS, NON-SI TO SI (METRIC) UNITS OF MEASUREMENT

Non-SI units of measurement used in this report can be converted to SI (metric) units as follows:

| Multiply | BY | To Obtain |
|---|---|---|
| cubic feet | 0.02831685 | cubic metres |
| degrees (angle) | 0.01745329 | radians |
| Fahrenheit degrees | 5/9 (F - 32) | Celsius degrees of Kelvins[1] |
| feet | 0.3048 | metres |
| pounds (force) | 4.448222 | newtons |
| pounds (force) per square inch | 0.006894757 | megapascals |
| pounds (mass) per cubic foot | 16.01846 | kilogram per cubic metre |
| seconds (angle) | 0.000004848 | radians |
| seconds (sidereal) | 0.9972696 | seconds |
| square feet | 0.09290304 | square metres |

[1] To obtain Celsius (C) temperature readings from Fahrenheit (F) readings, use the following formula: C = (5/9)(F - 32). To obtain Kelvin (K) readings, use: K = (5/9)(F - 32) + 273.15.

# CHAPTER I

# INTRODUCTION

## 1.1 OVERVIEW

The advantages of underground facilities for storage of explosives and ammunition include constant humidity and temperature conditions, and greater protection against enemy attack, fire, intrusion, or sabotage. However, the establishment of adequate safety standards (assuming accidental explosions in the magazines) must precede their use. These safety standards must identify the required depth of rock or soil cover, minimum spacing between storage chambers, and the minimum safe distance between the portal and inhabited buildings and/or public roads. These parameters are dependent upon the geologic media, underground geometrical configurations, type and quantity of explosive, and the topography outside the portal. Since the number of variables is extensive, a comprehensive analytical and experimental analysis of the problem is prohibitive. As a result, several aspects of the problem had not been investigated adequately at the time of this study.

The major portion of the work reported here was conducted in 1979-80, and the "previous" studies referred to in the text of this report were published prior to 1979.

## 1.2 BACKGROUND

In most instances, the greatest hazard from accidental explosions of deeply buried magazines is airblast. Consequently, previous investigators have addressed primarily the airblast standoff distance required for inhabited buildings. The general approach has been to obtain empirical mathematical relationships based upon small-scale model test data to predict the peak pressure generated at the portal of a particular geometry as a function of the explosive loading density of the magazine. Empirical relationships are then developed to predict the peak free-field pressures at scaled distances based upon the peak pressure at the portal. For the geometrical configuration and range of loading densities investigated, this predictive technique is adequate; however,

extrapolation of the empirical relationships to different geometries does not appear to be mathematically rigorous and may not produce valid estimates. These investigations will be discussed in more detail in Chapter 2.

The goal is to suppress the explosion and to reduce the standoff distance required for buildings as a result of the ground shock or airblast hazard. However, prior to this investigation, significant deficiencies existed in prediction of ground shock near decoupled[2] cylindrical cavities of finite length. The ground shock produced by decoupled cylindrical charges had been investigated only at large distances from the cavity. The effects of decoupling near a cavity had been investigated only for spherical geometries. As a result, the separation distances between storage chambers required to prevent explosive communication could not be determined accurately. Similarly, it was not possible to predict the chamber separation required to prevent an explosion in one chamber from damaging the contents of an adjacent chamber. Ideally, only minor surface damage to the wall of the nearest adjacent chamber should occur. And finally, additional information was needed in order to determine the safe standoff distance between underground magazines and residential buildings required to preclude structural damage as a result of ground motion.

## 1.3 OBJECTIVE

The general objective of this investigation was to improve the state-of-the-art of prediction techniques used for establishing underground explosive storage safety standards. Since the ground shock produced by decoupled explosions in cylindrical cavities was not well defined, emphasis was on determining standoff distances required to prevent explosive communication, separation required to minimize damage to contents in adjacent chambers, and safe standoff distances for ground shock effects on public buildings and highways. A secondary objective was to determine safe standoff distances for airblast propagating from the portal.

---

[2] A "decoupled" charge is defined as a cavity or chamber loaded with explosives which occupy less than the entire volume of the chamber.

## 1.4 APPROACH

The following approach was used to develop equations to predict safe standoff distances. First, literature germane to each major aspect of the problem was reviewed. The gas dynamics part of the problem included the peak pressure generated in vented and unvented cavities, blast propagation through tunnels and free-field blast propagation. The ground motion survey included analytical and experimental investigations of the strain and velocity fields produced by decoupled explosions in cavities in rock, and the analysis of the spall process at free rock surfaces. The literature survey is presented in Chapter 2.

Second, experimental data voids were identified which precluded an analysis of the cylindrical decoupling process. A small-scale model was designed and used to obtain the additional data required to predict the free-field strain and velocity field. Additionally, the model was designed to measure the free-field airblast pressures generated by the blast exiting the portal. The design of the model is discussed in Chapter 3.

Third, the data were analyzed and the ground shock propagation process was deduced for decoupled detonations in cylindrical cavities of finite length (Chapter 4). Equations were developed which express the relationship between free-field strain, the geometry of the cavity, the properties of the media and the loading density of the chamber.

Fourth, equations were developed to predict the respective ground shock standoff distances required. These equations were compared to those currently employed in the 1980 Department of Defense (DOD) Ammunition and Explosive Safety Standards (Reference 1). The details are presented in Chapter 5.

# CHAPTER 2
# LITERATURE REVIEW

Two major explosion phenomena--gas dynamics and ground shock--are relevant to the determination of standoff distances required for underground magazines. The gas dynamics area includes the detonation pressure generated in the storage chamber, attenuation of the shock front during propagation through the magazine complex, prediction of the blast pressure history at the portal, and the external, free-field decay of the blast wave. The ground shock area includes determination of the stress induced in the storage chamber walls, analysis of the free-field, and determination of the response of free surfaces as a function of the incident strain. Relevant literature in each of these areas will be discussed.

## 2.1 GAS DYNAMICS

2.1.1 Cavity Pressure. Explosions produce instantaneous release of tremendous amounts of energy. Strong shock waves quickly develop and interact with the cavity boundaries (Brode and Parkin, Reference 2). After numerous reflections and shock interactions, the waves are rapidly dissipated and a quasistatic pressure is generated, referred to here as the chamber pressure (Proctor 1972, Reference 3). The peak wall pressures developed by reflection of the initial shock can be significantly (8 to 10 times) larger than the chamber pressure (Skjeltorp, Hegdahl, and Jenssen, Reference 4). Although the reflected shocks have relatively small impulse, localized cracking of the chamber and nearby tunnel walls can be produced. In a closed cavity, the chamber pressure decays slowly as a result of heat loss to the walls. If the cavity is vented, the chamber pressure decay rate is controlled by the magnitude of the mass flux of the detonation products (Proctor, Reference 5).

Filler (Reference 6) developed a formulation to predict the chamber pressure, using an elementary energy balance which assumed that the ratio of specific heat was constant and that an oxygen-deficient condition did not exist. Consequently, this analysis was limited to low loading densities. For TNT, the technique is valid for chamber loading densities

less then 0.02 lb/ft$^3$. An empirical fit to experimental data for TNT was suggested by Weibul (Reference 7). However, the equation was limited to the range of the reported data, and there was not an effective means of relating TNT data to other explosives.

Theoretical techniques have also been developed to predict the chamber pressures generated by explosions in cavities. Proctor (1974, Reference 5) wrote a flexible computer code for explosives containing carbon, hydrogen, oxygen and/or aluminum. Based upon the chemical composition of the explosive and the quantity of air in the chamber, a chemical balance is used to determine the quantities of $Al_2$, $O_3$, $H_2O$, CO, $CO_2$, C, $H_2$, $O_2$, and $N_2$ that are generated by the chemical reaction. The amount of thermal energy (Q) generated by the reaction was then calculated. To facilitate computations, Proctor assumed that the mixture of detonation products was initially at ambient temperature and pressure. The thermal energy released by the reaction is added to the ambient condition by a constant volume process,

$$Q = \left(C_V\right)^T (T)\ dT$$

where $C_V$ is the specific heat of the gas at constant volume and T is the equilibrium temperature.

The integral equation is solved by iteration for the equilibrium temperature of the final mixture which satisfies the equation. Using the equilibrium temperature, mass of products, and the volume of the chamber, an equation of state was employed to calculate the chamber pressure. Figures 2.1 and 2.2 provide comparisons of Proctor's (1974, Reference 5) theoretical predictions with experimental data for TNT and PETN explosives. Stromsoe (Reference 8) calculated the temperature and chamber pressure developed in an unvented cavity by the detonation of TNT charges. For the range of loading densities investigated (0.012 to 16.88 lb/ft$^3$), his results were identical to Proctor's.

2.1.2 Blast Propagation in Tunnels. Following an explosion in an underground magazine, venting of the detonation products through the chamber entrance results in the propagation of shock waves through the

access tunnel. The physical phenomena involved are complex, and a generalized prediction of the blast pressures produced inside the tunnel or at the portal is very difficult.

First, consider the movement of the blast wave into the access tunnel from the storage chamber. Upon entering the tunnel, the peak overpressure is significantly reduced by diffraction (Porzel, Reference 9). As the shock front turns and the flow is accelerated, a pressure drop occurs. Diffraction is quickly followed by other irreversible losses. A few diameters inside the tunnel, the peak shock pressure increases over the diffraction pressure. This basically results from the interrelated process of preferential flow, multiple reflections and shocking up. Deeper in the tunnel (within approximately 20 diameters), the turbulent boundary layers of the shock front converge, and a turbulent choke develops. The turbulent choke is believed to form at a constant distance behind the shock front. The flow then becomes a quasi-steady state process.

The roughness of the tunnel wall surface also attenuates the peak blast pressures (Skjeltorp 1968, Reference 10). For a typical underground storage facility, surface roughness could reduce the pressure outside the portal by a factor of two (or more), compared to an essentially smooth-walled facility (Skjeltorp 1975, Reference 11). The degree of attenuation depends upon the shock strength, as well as the degree of surface roughness (Kriebel, Reference 12).

Porzel's theoretical analysis and several experimental investigations have demonstrated that macroscopic surface roughness in tunnels significantly attenuates weak shocks by surface friction. In contrast, strong shocks are relatively insensitive to macroscopic surface roughness. Even if there are no viscous losses to surface friction, attenuation in straight tunnels still occurs as a result of rarefaction. Advancement of the rarefaction wave toward the shock front results in a reduction of the peak pressure and an increase in the duration of the positive phase. Data from model tests have quantified this effect as a function of tunnel length (Schmidt, Reference 13).

Many underground storage complexes are much more complicated than a single storage chamber connected to a straight access tunnel. Each bend, corner, or intersection in a tunnel constitutes a geometrical discontinuity which impedes shock propagation by producing multiple shock reflections. In general, the more complex the geometry, the greater the attenuation of the blast pressure as it propagates through a tunnel.

Theoretically, blast pressures generated in an underground tunnel complex can be described mathematically and predicted numerically (Skjeltorp, Hegdahl, and Jenssen, 1975, Reference 4). In most studies to date, however, the approach has been to determine experimentally the blast pressures generated in small-scale models of the particular geometry of interest. Semi-empirical equations are fit to the measured peak, side-on pressure data obtained for a particular geometry, such as that shown in Figure 2.3. According to Skjeltorp (1968, Reference 10), for a storage chamber connected to a single access tunnel, the relationship between peak pressure, charge weight in the magazine, and dimensions of the complex is

$$P = 953 \left(\frac{Q}{V_t}\right)^{0.61} \left(\frac{A_j}{A_c}\right)^{0.19}, \quad 0.11 \leq \left(\frac{A_j}{A_c}\right) \leq 0.45 \qquad (2.1)$$

where P is peak side-on pressure (psi)

Q is total equivalent TNT charge weight (lbs)

$A_j$ is the cross-sectional area of the access tunnel ($ft^2$)

$A_c$ is the area of the storage chamber ($ft^2$)

and $V_t$ is the total volume ($ft^3$) of the chamber and tunnel segment to the point of interest

Peak pressure attenuation rates have been investigated for several basic tunnel designs (Skjeltorp, et al, 1975, Reference 4). The lumped approach shown above illustrates the approach used in most experimental studies. The loading densities of the storage chambers investigated have been less than 6.3 $lb/ft^3$, with most less than 3.25 $lb/ft^3$.

This method produces very good results for the geometry investigated but has several limitations, according to Skjeltorp (Reference 4). The

data obtained is applicable only to geometrically similar models (or full-scale designs), and only for the range of loading densities that were investigated.

2.1.3 Free-Field Blast Pressure. An accidental explosion in an underground magazine normally produces a hazardous blast wave that propagates outward from the tunnel exit. This external blast wave attenuates at different rates according to direction from the exit; i.e., as a function of angular departure from the extended tunnel center line. Generally, hazardous airblast effects will extend much farther from the exit portal than will the detrimental effects of ground shock or debris. The minimum safe distance (or airblast standoff distance) is usually defined as the distance from the portal to a point at which the overpressure is equal to 0.725 psi (Skjeltorp, Reference 4).

The airblast standoff distance, for a given pressure criterion, is usually predicted from empirical relations which describe the attenuation of the peak pressure exiting the tunnel portal; i.e., the exit pressure. Fredrickson and Jenssen (Reference 14) obtained free-field airblast data from small-scale model tests where the access tunnel exited onto a 30-degree (downward) slope. Based upon these results, they proposed the empirical relationship

$$d_c = k_\theta P_o^{0.67} \tag{2.2}$$

where $d_c$ is the airblast standoff distance

$P_o$ is the overpressure at the tunnel exit

$k_\theta$ is a constant determined by the geometrical design of the complex and direction of interest outside the tunnel.

Fredrickson and Jenssen noted that the technique may not yield accurate quantity distances for other geometrical configurations. Skjeltorp (1975, Reference 4) subsequently reviewed Fredrickson and Jenssen's data and proposed the empirical equation

$$\frac{r}{D_T} = C_\theta P_o^{0.67} \tag{2.3}$$

where r is the radial distance in feet from the portal, along a radial line originating at the portal to a point at which the peak blast pressure has decayed to 0.725 psi.

$D_T$ is the diameter of the access tunnel

$C_\theta$ is a directional coefficient functionally dependent upon the direction of measurement with respect to the extended centerline

and $\theta$ is the angle between the direction of the extended centerline.

The values of $C_\theta$ as a function of $\theta$ are:

| $\theta$(deg) | 0 | 30 | 60 | 90 | 120 |
|---|---|---|---|---|---|
| $C_\theta$ | 3.00 | 2.67 | 2.00 | 1.33 | 0.75 |

Skjeltorp suggests that Equation 2.3 is valid for any underground geometry if the exit geometry is equivalent to that used by Fredrickson.

In a study involving a dual storage chamber design, Gurke and Scheklinski (Reference 15) obtained free-field blast data along the extended centerline of the main access tunnel. The model was fabricated from steel tubes which exited onto a flat surface (0-degree exit surface). At low loading densities, the peak blast pressures were substantially lower than those predicted by Equation 2.3. At larger loading densities (1.0 to 2.5 $lb/ft^3$), the blast data obtained along the extended centerline access agreed with Equation 2.3. Thus, the rate of decay along the extended centerline was not affected by exit slopes between 0 and 30 degrees. These results provided no additional information about the directional sensitivity of Equation 2.3 to the exit geometry. The blast pressures generated along the extended centerline should be less sensitive to the exit geometry than any other direction.

Several investigations have been conducted to determine the external, free-field blast pressures generated by gun firings. Westine (Reference 16) reviewed data obtained over a wide range of operating conditions, from fourteen different weapons. The barrel lengths and bore diameters varied more than an order of magnitude. The total energy of the propelling charges varied by a factor of 4490. Peak free-field blast data were obtained along radial lines in a horizontal plane that was an

extension of the bore. Each of the measurements made along 30 to 90-degree lines showed the peak blast pressure decaying approximately as $r^{-3/2}$.

A comparison of the results obtained by the various investigators (Skjeltorp, Fredricksen, Jenssen, Gurke, Scheklinski, and Westine) suggests that the directional coefficients in Equation 2.3 in the 30, 60 and 90-degree directions are not sensitive to differences in exit slopes between 0 and 30 degrees.

## 2.2 GROUND SHOCK

It has been shown both theoretically (Herbst, Werth, and Springer, Reference 17) and experimentally (Perret, Reference 18) that decoupling the explosive energy by detonating charges in cavities larger than the charge volume is an effective method of reducing ground shock magnitudes. The decoupling in spherical cavities, for example, has been explored as a possible method for concealing underground nuclear explosions. The technique is also used in the blasting industry in presplitting, smooth wall, and cushion blasting operations.

Since munitions and explosives typically occupy only a few percent of the total volume of underground magazines, the net explosive weight of an accidental explosion would be comparable to a concentrated charge that is highly decoupled. Thus, the amount of decoupling is inversely proportional to the magazine loading density.

Decoupling should result in much less energy coupled into the earth by accidental explosions in magazines than would be predicted based on data from fully-coupled tests. Theoretical investigations of decoupling in cylindrical cavities have not been published. However, empirical data (Atchison, Duvall, and Pugliese, Reference 19) were obtained for radial distances greater than 10 cavity lengths, for matching decoupled and fully-coupled cylindrical charge detonations. Drake (Reference 20) demonstrated that, at these ranges, the reduction in ground shock achieved by decoupling cylindrical charges is roughly equivalent to that of spherical charge decoupling. The peak particle velocity obtained for decoupled charges (v) divided by the peak particle velocity obtained for fully coupled charges ($v_o$), expressed as a function of the relative

loading density, is shown in Figure 2.4. The data for granite and limestone were obtained using cylindrical cavities containing chemical explosives. Data for spherical cavities in salt involved both chemical and nuclear explosives.

The velocity and strain fields produced near fully-coupled cylindrical charges have not been reported. A small quantity of close-in data from decoupled cylindrical charges is available from the CIST program (Amend, References 21 and 22). In this program, a 5-lb/ft linear charge was detonated in 2-ft diameter vertical holes drilled through layered media. Peak particle velocities were obtained in each layer at radial distances of 1.5 to 6 cavity diameters. Five peak particle velocity measurements were obtained in sandstone, and six in granite.

The quantitative behavior of the peak strain (or particle velocity) around the detonation of linear charges in rock can be deduced. Near a linear charge of length L, the stress (or strain) field along the length of the charge is determined by cylindrical wave propagation. As the cylindrical wave advances, the amplitude of the wave front decays as $r^{-1/2}$, where r is the radial distance from the center of the charge (Persen, Reference 23). At large distances from a linear charge (i.e., where r>>L), the stress field approximates that produced by a spherical charge. Ideally, the amplitude of spherical waves decays as $r^{-1}$. However, as a result of irreversible losses (heat, mechanical crushing, etc.), the decay in rock is more nearly proportional to $r^{-2}$ (Cooper, Reference 24). As indicated in Figure 2.5, between those limits, a transition from cylindrical to spherical decay must occur.

2.2.1 Tunnel Damage. Underground installations can be significantly damaged by the stress waves generated from explosions within the facility. The magnitude of damage is dependent on the energy released by the charge, the degree of charge coupling (loading density), properties of the medium, and the distance between the charge and adjacent tunnels. Several investigations have been conducted to determine the strain (or velocity) threshold at which various types of tunnel damage occurs. Damage to tunnels is generally divided into four categories, based upon the damage profile (see Figure 2.6) along the tunnel wall nearest the charge. In Army nuclear weapons effects manuals (e.g., Reference 27),

the four zones (1, 2, 3 and 4) are called the zone of complete damage, the zone of rock breakage, the zone of continuous slabbing, and the zone of discontinuous damage, respectively.

The Underground Test (UGT) Program (Engineering Research Associates, References 28 and 29) provided damage data in three types of rock (limestone, granite and sandstone). The tunnels, in jointed granite and sandstone, had horseshoe-shaped cross-sections. The diameters of the tunnels tested were 6, 15, and 30 ft. Fully-coupled TNT charges, varying in weight from 320 to 32,000 pounds, were detonated at various distances from the test tunnel.

In addition, a series of 153 model tests were conducted at the Waterways Experiment Station in rock-matching grout having nominal unconfined compressive strengths of 10,000, 4,000 and 500 psi (Joachim, Reference 30). Various standoff distances and tunnel diameters were also tested in these models. Hendron, Clark, and Strange (Reference 31) used a model which had eight tunnels of various diameters oriented about a 2-lb TNT spherical charge. The distances from the center of the charge to the centerline of the tunnels ranged from 1 to 5 ft. Other data were obtained in a series of 23 tests conducted in Kayenta sandstone near Grand Junction, CO. Core samples indicated a relatively uniform rock with thin, horizontal, irregularly spaced, clay seams (Swift, Reference 32). Stemmed charges were detonated at various distances from 2, 3, and 4-ft diameter drill holes.

Based upon the results of these investigations, the following conclusions are implied: Zone 1 failure occurs when the compressive stress exceeds the ultimate compressive strength of the partially-confined medium adjacent to the opening; this usually corresponds to a strain of 0.5 to 1.0 percent. Zone 2 failure occurs when the local compressive strain around the opening equals the strain at ultimate conditions in partially-confined compression. For most rocks, this corresponds to a strain between 0.2 and 0.4 percent. Zone 3 damage occurs when the local compressive strain around the opening exceeds the strain corresponding to the ultimate strength in unconfined compression. Typically, this strain is between 0.06 and 0.2 percent. Zone 4 damage develops when the local tensile strain around the opening equals the

strain corresponding to the effective tensile strength of the rock. For most types of rock this type damage would occur at free-field strains of 0.03 to 0.06 percent.

2.2.2 Spall. The conditions under which spalling occurs are well understood (Rinehart, Reference 33). When a compressional wave intersects a free surface, it will be reflected as a tension wave, and the total stress at a point in the rock wall will be the sum of the incident compressional stress and the reflected tension stress. Whenever the tension exceeds the compression by an amount approximately equal to the ultimate tensile strength of the rock, it will fracture and a spall will develop. The velocity of the spall will depend upon the magnitude of the momentum trapped within the spall.

If the net stress level is greater than twice the ultimate tensile strength of the rock, multiple spalls will develop. Assume that the first spall was created as indicated above. The remaining part of the compressional wave will strike the new free surface, and the process will be repeated until the amplitude of the tensile stress is less than the ultimate tensile strength of the rock.

Fractures in the medium may significantly affect spalling (Reference 33). If the fractured surfaces are in intimate contact; a compression wave can be transmitted through the interface with little or no degradation; however, the interface cannot support tension. When the reflected tensile wave from a free surface returns to the fracture, a spall will occur at the fracture. The velocity of the spall will depend upon the momentum trapped within the spalled slab of rock, which is dependent on the slab thickness.

Spalling in real materials is often complicated by attenuation, divergence, inhomogeneities in the material and finite fracture times. Spall velocity predictions are often based upon idealized assumptions. In a safety analysis, this is not practical because the conditions at the free surface are not always known, and upper bound predictions may not result. It appears more realistic to specify the required separation of underground storage chambers in terms of the maximum possible spall velocity, which is always equal to or less than twice the particle velocity at the free surface.

## 2.3 SUMMARY (Literature Review)

The interrelated processes that govern the effects of explosions in underground magazines have not been sufficiently investigated to establish comprehensive safety standards. Theoretical techniques have been developed to accurately predict the pressure generated by explosions in underground chambers. Peak blast pressures produced in the connecting passageways and at the portal can be predicted empirically, but only for the limited number of geometries and loading densities that have been tested.

The ground shock produced by decoupled explosions in cylindrical cavities also has not been adequately investigated. It has been demonstrated that decoupling will significantly reduce the peak strain and velocity field. Near cylindrical cavities of finite length, where ($r \ll L$), the decay in the peak values near the cavity will be dictated by cylindrical wave expansion. Far from the cavity, where ($r \gg L$), spherical wave expansion will predominate. The radial distance at which cylindrical decay changes to spherical has not been determined experimentally. Consequently, the close-in stress and strain fields cannot be predicted with any degree of certainty.

The magnitude of damage to unlined tunnels as a result of the stress field generated by an external explosion can be related to the strain developed at the tunnel wall. In unlined tunnels, catastrophic failure (tunnel closure) may occur if the strain at the tunnel wall is greater than 0.4 percent. Catastrophic wall failure of a magazine could conceivably result in explosive initiation of the contents. Minor surface damage may occur at strain magnitudes greater than 0.03 percent. To preclude damage to the contents of adjacent underground storage chambers, the chamber separation should be large enough to prevent any wall surface damage in the chambers adjacent to an explosion.

From the literature survey, it was apparent that a major problem exists in the current ability to predict the magazine spacings required to prevent interchamber damage by ground shock. No close-in ground shock data are available for decoupled, cylindrical cavities. A small-scale model test program was therefore designed to obtain such data as a part of this study.

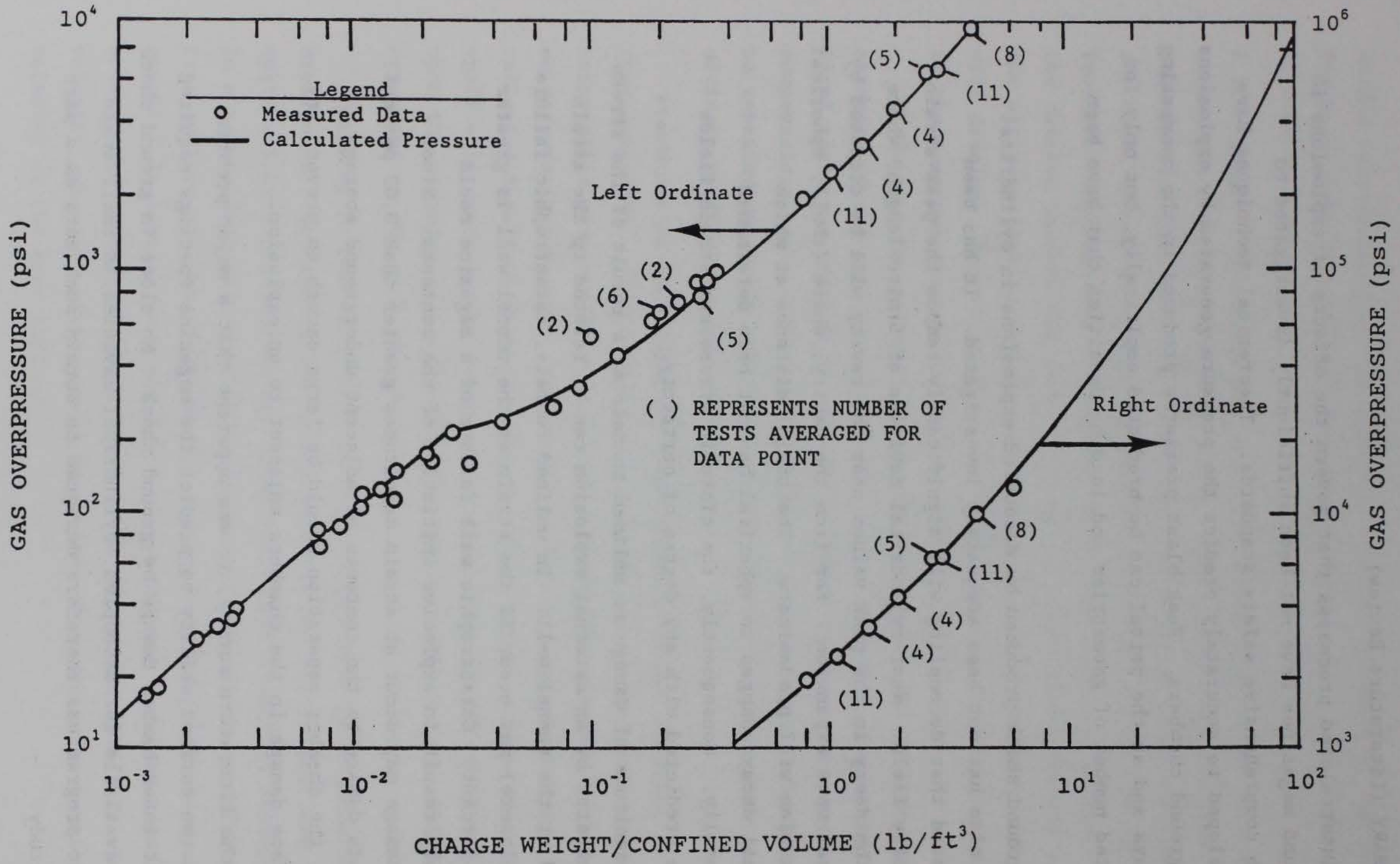


Figure 2.1. Comparison of calculated (curves) versus measured values of confined explosion gas pressure for TNT in air at sea level (Proctor 1974, Reference 5).

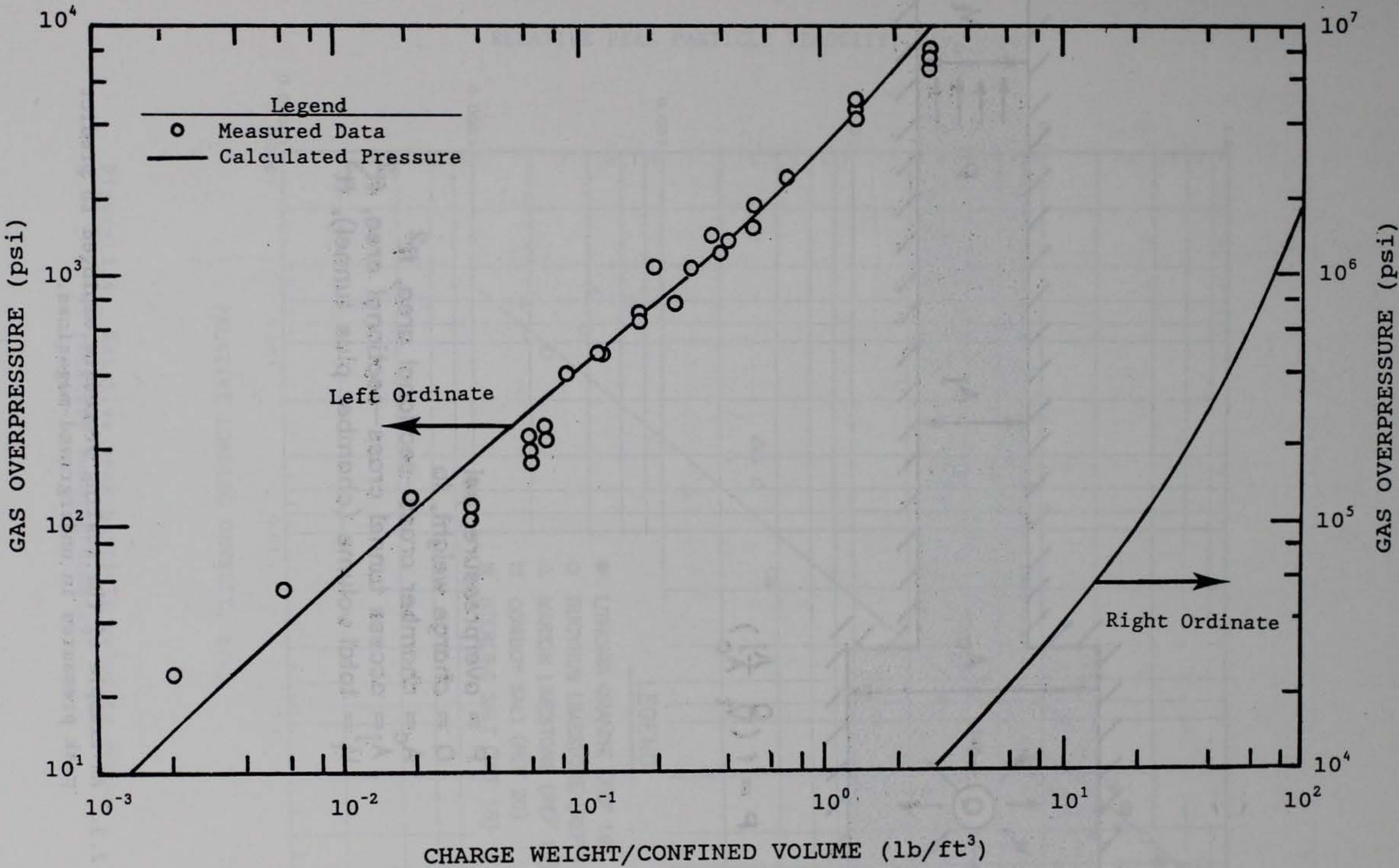


Figure 2.2. Comparison of calculated (curves) versus measured values of confined explosion gas pressure for PETN in air at sea level (Proctor 1974, Reference 5).

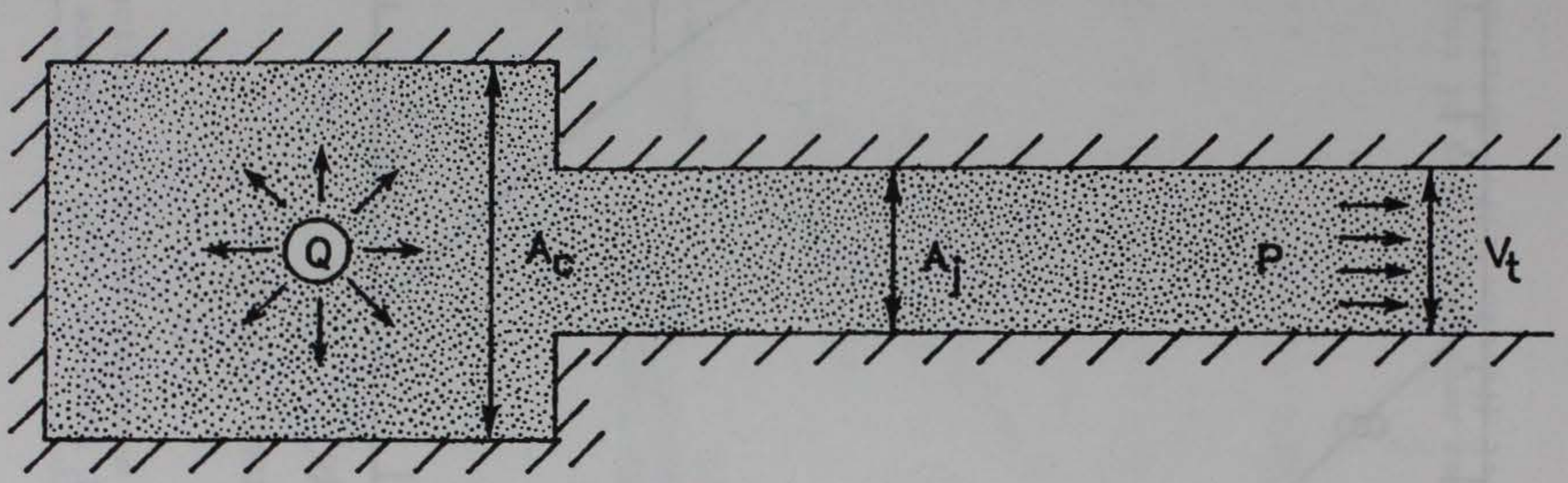


$$P = f\left(\frac{Q}{V_t}\ \frac{A_j}{A_c}\right)$$

P = overpressure, psi
Q = charge weight, lb
$A_c$ = chamber cross-sectional area, $ft^2$
$A_j$ = access tunnel cross-sectional area, $ft^2$
$V_t$ = total volume (chamber plus tunnel), $ft^3$

Figure 2.3. An example of the scaling procedure employed to predict peak pressures in underground magazines.

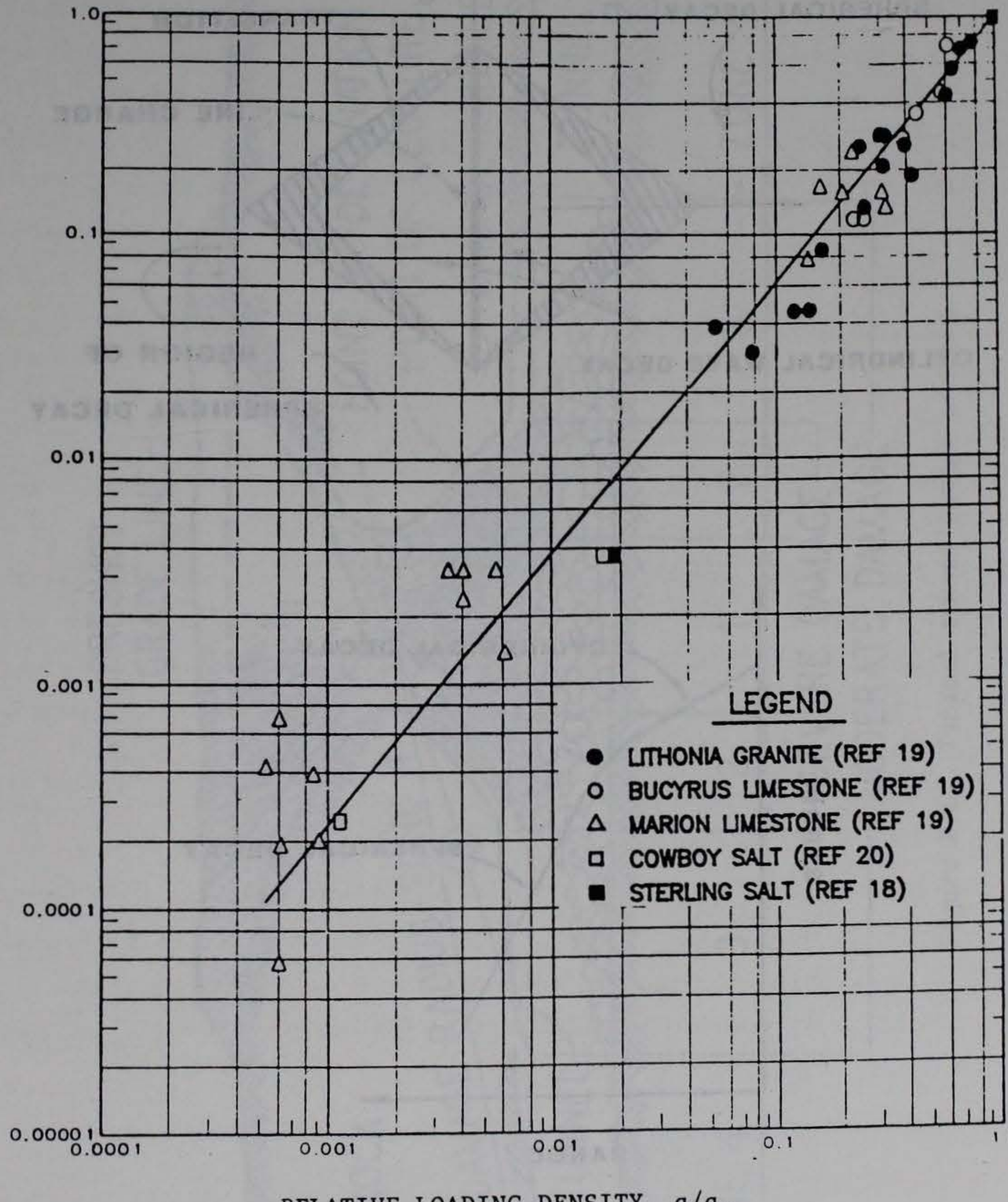


Figure 2.4. Relative peak particle velocity versus relative loading density.

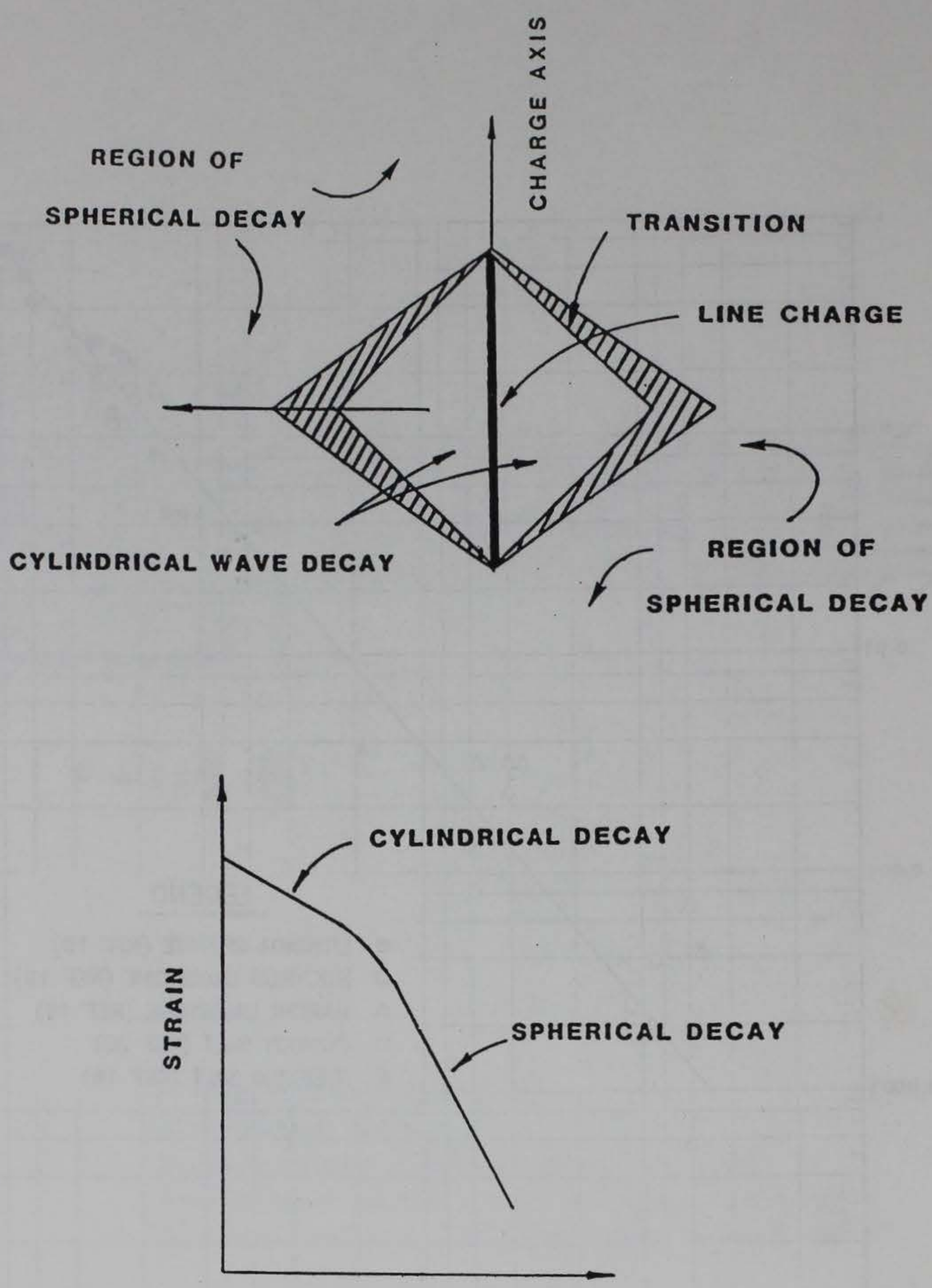


Figure 2.5. Qualitative behavior of the strain field produced around line charges of finite length.

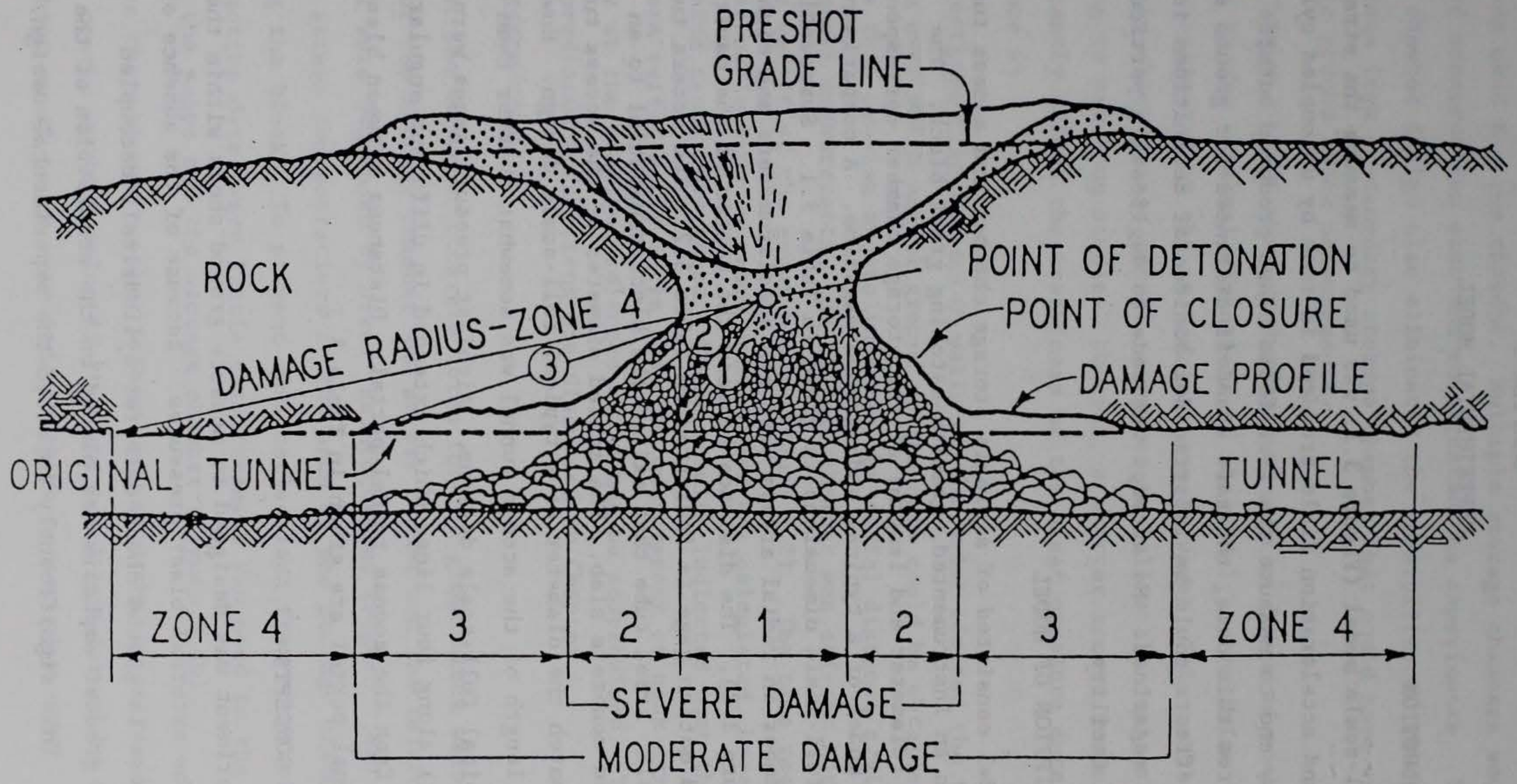


Figure 2.6. Typical tunnel damage profile.

# CHAPTER 3

# EXPERIMENTAL MODEL

## 3.1 INTRODUCTION

A small-scale model (Figure 3.1) was used to measure the strain, velocity and acceleration field produced in rock by uncoupled cylindrical explosions, and to measure the free-field blast produced outside the portal. From this data, the safe standoff distances for ground shock and air blast effects could be inferred for accidental detonations in full-scale magazines. No attempt was made to duplicate a particular full-scale facility.

## 3.2 DESCRIPTION OF MODEL

The model consisted of a single storage chamber and access tunnel embedded in an instrumented, granite-matching grout block. The dimensions (diameter and length) of the storage chamber correspond to a 1:75-scale model of a typical underground magazine. A comparison of the model and full-scale dimensions is given in Table 3.1. Surrounding the storage chamber in radial arrays were six accelerometers and eight strain gages (Figure 3.2). The distance between the center of the cavity and each ground motion gage is indicated in Table 3.2. The access tunnel was a smooth-wall, steel tube that exited the block tangential to an instrumented concrete slab. The scaled diameter of the access tunnel was chosen to match the diameter of a typical full-scale design. However, the scaled length of the access tunnel was somewhat shorter than those used in typical full-scale designs. Airblast pressure gages were placed (Figure 3.3) along four lines which extended in different angular directions from the access tunnel portal. Distances between blast gages and the tunnel portal are given in Table 3.3.

## 3.3 DESIGN CONCEPTS

The experiment was designed to measure ground shock within the grout block and the external blast pressures. Because of the absence of existing close-in ground shock data for cylindrical, decoupled explosions, greater emphasis was placed on the acquisition of the ground shock data. This significantly impacted the experimental design.

The relatively simple geometry of a single storage chamber and access tunnel was used for two reasons. Multiple storage chambers would have increased construction cost and complicated the experiments. The single storage chamber design also eliminated the possibility of wave reflections from a secondary storage chamber that could have compromised the basic ground shock measurements.

The length of the storage chamber was made as large as possible, relative to the external dimensions of the model, to maximize the radial distance dominated by the cylindrical stress wave. This resulted in a relatively short access tunnel, compared to full-scale designs. According to previous studies, however, a shorter access tunnel would not significantly affect the usefulness of the blast pressure data (Reference 4).

Reflections from the outer walls of the model limited the time duration over which useful ground motion data could be obtained. To minimize this problem and to increase the radial distance available for ground shock measurements, the storage chamber was off-set horizontally from the center of the grout block (Figure 3.2). The time required for the first reflection to reach each sensor was calculated, based on the anticipated grout wave speed. These results indicated that the transit times were sufficiently large that the measurement of peak strain or velocity at the stations selected would not be compromised. The accuracy of the predicted reflections are discussed in Chapter 4.

## 3.4 CONSTRUCTION

After the exterior concrete forms for the grout block were set, the forms for the storage chamber and access tunnel and the reinforcement material were suspended by wire. Reinforcement (Figure 3.4a) was used to prevent stress concentrations at the ends of the storage chamber from cracking the block. To prevent wave reflections from compromising the ground motion data, very little reinforcement was used in the region between the gages and the storage chamber (Figure 3.4b).

Since thermodynamic calculations indicated that massive, internal thermal cracks would develop if the test block was formed by a single pour, three equal pours were made on three consecutive days. Samples

were taken during each pour for later laboratory testing to confirm the properties of the grout. The sequence of the pours is shown in Figure 3.4. Prior to the second and third pours, the previous pour was coated with epoxy to minimize the effects of cold joints. During the second pour, thin-wall copper tubes (Figure 3.4c) were inserted for later gage placement. To insure bonding of the strain gage assembly to the test block, the vertical tube over the center of the storage chamber was removed after the third pour reached an initial set. The vertical holes were filled with same grout mix used to fabricate the test block. The accelerometers and strain gage column were then inserted into the wet grout-filled holes and the displaced grout was removed. For the vertical gage line, four strain gages were placed in the second and four in the third pours.

The exterior concrete slab was carefully constructed to minimize shock attenuation or reflection for the air blast gages. After pouring, the surface was polished to minimize surface roughness. The pressure gage canisters were installed with their tops flush with the slab surface. Care was taken to eliminate any surface irregularities near the concrete-canister interface.

## 3.5 INSTRUMENTATION

The selection of airblast gages was based predominately on the expected frequency and amplitude of the data. Sufficient blast data (discussed earlier) were available to predict both parameters. However, an additional constraint was imposed. It was expected that dilatation of the storage chamber model would impose a lateral acceleration to the blast slab. Thus, the pressure sensors needed to have negligible lateral acceleration sensitivity. As indicated in Table 3.4, the manufacturer's specifications indicated that the PCB pressure gages met these requirements. The pressure gages were mounted in waterproof, shock-isolation canisters. The sensing surface of each gage was slightly recessed. The recessed region (approximately 0.06 in.) was filled with silicone rubber to minimize light and thermal sensitivity.

The accelerometers were selected based on an extrapolation of spherical and cylindrical decoupling data (discussed earlier). The manufacturer's specifications for these gages are presented in Table 3.5. The accelerometers were placed in high-strength, watertight canisters. The lowest natural frequency of the canister was experimentally determined to be 32,000 Hz, which was compatible with the frequency response of the recording system. The mounting base was sufficiently strong to eliminate any base-induced strain which would degrade the accelerometer signal.

To measure strain, eight waterproofed strain gages were bonded to a 1.875-inch diameter grout column. The strain gages were 1/4-inch, 350-OHM gages with a gage factor of 2.14 at 75 degrees F. The grout column was made from the same mix used in the model to insure matching properties. The properties of the grout are given in Table 3.6.

## 3.6 DESCRIPTION OF THE CHARGE

The energy source used in all tests was Pentereythuital tetranitrate (PETN), with the trade name Primacord. PETN has several advantages. It was readily available in strands of various linear densities. As a result, a linear charge could be assembled easily by varying the number and the density of the strands. The burn rate (26,200 ft/sec) was fast enough to effectively produce a cylindrical ground shock. Additionally, experimental data and the theoretical techniques were available to accurately predict the equilibrium pressure developed in the storage chamber by detonation of the PETN (Figure 2.2).

The charges were assembled by taping the required number of strands together. The charges were detonated at the portal ends. The smallest and largest charges used in the test program are shown in Figure 3.5.

## 3.7 PROCEDURE

The following procedure was used for each test:

a. The sensors were calibrated.

b. The charge was assembled and placed in the test fixture.

c. The tape machines were started.

d. The charge was fired and the data recorded.

e. The test fixtures were cleaned for the next test.

## 3.8 TEST PROGRAM

The test program was performed in three phases. Phase 1 was designed primarily to obtain ground shock data; however, one or more airblast stations were monitored during each test. Phase I consisted of the following tests:

| Number of Tests | Loading Density $lb/ft^3$ | Loading Density $kg/m^3$ |
|---|---|---|
| 4 | 0.1 | 1.6 |
| 4 | 0.3 | 4.8 |
| 4 | 1.0 | 16.0 |
| 3 | 2.0 | 32.0 |

Several tests were conducted at each loading density to establish the reproducibility of the data. The loading density is the total charge weight divided by the volume of the storage chamber. To make sure that the accelerometers and strain gages were appropriately ranged, the loading densities were gradually increased during the series.

Phase 2 was designed to obtain airblast pressure data outside the tunnel. It consisted of a total of 51 tests conducted at five loading densities, ranging between 0.1 and 0.46 $lb/ft^3$. Low loading densities were used initially to prevent damage to the model. This phase consisted of the following tests:

| Number of Tests | Loading Density $lb/ft^3$ | Loading Density $kg/m^3$ |
|---|---|---|
| 14 | 0.1 | 1.6 |
| 13 | 0.2 | 3.2 |
| 15 | 0.28 | 4.5 |
| 6 | 0.37 | 6.0 |
| 3 | 0.46 | 7.4 |

Phase 3 consisted of a single test at a loading density of 25.3 $lb/ft^3$ (405 $kg/m^3$). Catastrophic failure of the model was anticipated;

however, peak strains were measured successfully, since the breakup and mass motion of the block occurred after passage of the incident stress wave.

## 3.9 DATA ACQUISITION AND REDUCTION

The data were recorded on a 14-track FM analog tape machine operating at a tape speed of 120 in./sec. The frequency response of the recording system was 40 KHz, which was consistent with the frequency response of other system components. The analog data were digitized on an analog-to-digital converter, recorded on magnetic tape, and subsequently processed through the WES GE-635 computer. Velocity histories were obtained by numerical integration of the acceleration histories. Typical plots of velocity, strain and pressure histories are presented in Figures 3.6, 3.7, and 3.8, respectively (note that negative strains are compressive on all records). A typical strain history obtained at a loading density of 25.3 $lb/ft^3$ is presented in Figure 3.9. Peak velocity, strain and pressure data were obtained from these records and are recorded in Tables 3.7, 3.8, and 3.9, respectively. These results are analyzed in Chapter 4.

Table 3.1 Design Parameters for 1:75 Scale Model and Full-Scale Underground Storage Facility

| Parameter | Model | Full-Scale |
|---|---|---|
| Access Tunnel Length | 3.5 ft | 262.5 ft |
| Access Tunnel Diameter | 0.223 ft | 16.7 ft |
| Storage Chamber Diameter | 0.318 ft | 23.8 ft |
| Storage Chamber Length | 3.76 ft | 282 ft |
| Storage Chamber Volume | 0.298 $ft^3$ | 125,550 $ft^3$ |
| Charge Mass for Loading | 0.744 lb | 313,875 lb |

Table 3.2 Distance Between the Center of the Storage Chamber and Ground Motion Gages

| Accelerometers | | Strain Gages | |
|---|---|---|---|
| Gage Number | Distance ft | Gage Number | Distance ft |
| 1 | 1.65 | 8 | 1.13 |
| 2 | 3.03 | 9 | 1.46 |
| 4 | 4.96 | 10 | 1.79 |
| 5 | 1.38 | 11 | 2.13 |
| 6 | 1.93 | 12 | 2.46 |
| 7 | (deleted) | 13 | 2.79 |
| | | 14 | 3.13 |

Table 3.3 Location of Airblast Measurement Stations with Respect to the Portal and the Extended Tunnel Centerline

| Station Number | Angle with Respect to the Extended Center line degrees | Radial Distance From Tunnel Portal ft |
|---|---|---|
| 1 | 0 | 0.75 |
| 2 | 0 | 1.50 |
| 3 | 0 | 2.50 |
| 4 | 0 | 10.00 |
| 5 | 30 | 3.00 |
| 6 | 30 | 5.00 |
| 7 | 30 | 8.00 |
| 8 | 45 | 2.00 |
| 9 | 45 | 3.50 |
| 10 | 45 | 5.00 |
| 11 | 45 | 7.00 |
| 12 | 60 | 1.00 |
| 13 | 60 | 2.50 |
| 14 | 60 | 5.00 |

Table 3.4 Manufacturer's Specifications for Pressure Sensors

| | |
|---|---|
| Sensitivity | 50 mV/psi |
| Resolution | 0.004 psi |
| Resonant Frequency | 250,000 Hz |
| Rise Time | 2 micro-seconds |
| Time Constant | 1 sec |
| Low Frequency (5% down) | 1 Hz |
| Linearity | 1 percent |
| Range (for 5 volts out) | 100 psi |
| Range (for 10 volts out) | 200 psi |
| Maximum Pressure | 1000 psi |
| Output Impedance | 100 ohms |
| Vibration/Shock | 2,000/20,000 g |
| Acceleration Sensitivity | 0.002 psi/g |
| Temperature Range | -100 to +270 F |
| Temperature Coefficient | 0.03% F |
| Flash Temperature | 3000 F |

Table 3.5 Manufacturer's Specifications for Accelerometers

| | | | | |
|---|---|---|---|---|
| Range, g pk | ±5,000 | ±10,000 | ±20,000 | ±50,000 |
| Sensitivity, mV/g, at 10 Vdc, Nominal value: | 0.100 | 0.050 | 0.025 | 0.010 |
| Minimum value: | 0.075 | 0.037 | 0.018 | 0.007 |
| Mounted Resonance Frequency, Hz, nominal | 50,000 | 70,000 | 100,000 | 180,000 |
| Useful Frequency Response, Hz, | 8,000 | 9,000 | 12,000 | 30,000 |
| Environmental Acceleration Limits (Sensitive Axis, g pk) | ±12,500 | ±25,000 | ±50,000 | ±100,000 |
| Transverse Axis, g pk | ±12,500 | ±25,000 | ±30,000 | ±50,000 |
| Minimum Half-Sine Pulse Duration, microseconds | 125 | 90 | 65 | 30 |

Table 3.6 Experimentally-Determined Grout Properties
(average values from six specimens)

| | |
|---|---|
| Specific Gravity | 2.19 |
| Compressional Wave Velocity (ft/sec) | 12,954 |
| Shear Wave Velocity (ft/sec) | 8,373 |
| Shear Wave Velocity/Compressional Velocity | 0.647 |
| Young's Modulus (psi) | $4.727 \times 10^6$ |
| Shear Modulus (psi) | $2.071 \times 10^6$ |
| Bulk Modulus (psi) | $2.201 \times 10^6$ |
| Lame Constant (psi) | $8.205 \times 10^5$ |
| Poisson's Ratio | 0.140 |

Table 3.7 Peak Velocities Obtained as a Function of Loading Density and Range

| Loading Density lb/ft$^3$ | Peak Particle Velocity, ft/sec | | | | | |
|---|---|---|---|---|---|---|
| | Range, ft | | | | | |
| | 0.826 | 1.378 | 1.652 | 1.927 | 3.029 | 4.958 |
| 0.1 | 0.46 | 0.23 | 0.2 | ---- | 0.04 | 0.032 |
| 0.1 | 0.62 | 0.18 | 0.29 | ---- | 0.07 | 0.05 |
| 0.1 | 0.28 | 0.36 | 0.13 | 0.18 | 0.028 | 0.03 |
| 0.3 | 1.0 | 0.7 | 0.56 | ---- | 0.18 | 0.1 |
| 0.3 | 1.4 | 0.72 | 0.62 | 0.38 | 0.25 | 0.16 |
| 0.3 | 1.2 | 0.75 | 0.71 | 0.45 | 0.22 | 0.15 |
| 0.3 | 1.0 | 0.72 | 0.45 | 0.37 | 0.2 | 0.12 |
| 1.0 | 3.2 | 2.4 | 1.1 | 1.0 | 0.7 | 0.23 |
| 1.0 | 3.5 | 1.6 | 2.0 | 1.45 | 0.6 | 0.2 |
| 1.0 | 4.9 | 3.0 | 1.2 | 1.6 | 0.25 | 0.28 |
| 1.0 | 4.8 | 2.0 | 1.7 | 2.6 | 0.55 | ---- |
| 2.0 | 11.6 | 4.5 | ---- | ---- | ---- | 1.2 |
| 2.0 | 11.0 | 6.5 | 7.0 | 7.2 | 3.6 | 1.3 |
| 2.0 | 11.0 | 6.5 | 9.0 | 7.0 | ---- | 2.3 |

Table 3.8 Peak Strain Obtained as a Function of Loading Density and Range

| Loading Density lb/ft$^3$ | Peak Strain, μin./in. | | | | | | | |
|---|---|---|---|---|---|---|---|---|
| | Range (ft) | | | | | | | |
| | 0.792 | 1.125 | 1.458 | 1.792 | 2.125 | 2.458 | 2.792 | 3.125 |
| 0.1 | 54 | 69 | 38 | 40 | 33 | 23 | 23 | 16 |
| 0.1 | 40 | 78 | 25 | ---- | ---- | ---- | ---- | ---- |
| 0.1 | 40 | 107 | 30 | 37 | 20 | 14 | ---- | ---- |
| 0.1 | 34 | 20 | 20 | 12 | 18 | 13 | 8 | 8 |
| 0.3 | 119 | ---- | 86 | 49 | 52 | 53 | 22 | 12 |
| 0.3 | 97 | 94 | 43 | 33 | 33 | 27 | 25 | ---- |
| 0.3 | 119 | 109 | 102 | 63 | 61 | 54 | 41 | 33 |
| 0.3 | 139 | 130 | 95 | 57 | 63 | 55 | 44 | 48 |
| 1.0 | 373 | 224 | 261 | ---- | 71 | 41 | 39 | 28 |
| 1.0 | 240 | 229 | 155 | ---- | 54 | 42 | 24 | 26 |
| 1.0 | 310 | 271 | 206 | 44 | 32 | 22 | 30 | 21 |
| 1.0 | 347 | 237 | 250 | 47 | 43 | 58 | 25 | 31 |
| 2.0 | 560 | 626 | 465 | 224 | 149 | 86 | 70 | 68 |
| 2.0 | 772 | ---- | 633 | 291 | 290 | 145 | 137 | 63 |
| 2.0 | 984 | 956 | 767 | 528 | ---- | ---- | ---- | ---- |
| 25.3 | ---- | ---- | 7000 | 7100 | 7800 | 4985 | 3850 | 2420 |
| 25.3 | ---- | ---- | 9000* | 5800* | 5900* | 4800* | ---- | ---- |

* Obtained from a second strain gage column used only for that test.

Table 3.9a Peak Blast Pressures Measured Along the 0-Degree Line (Extended Centerline of the Access Tunnel)

| Loading Density $lb/ft^3$ | Radial Distance ft | Peak Pressure psi |
|---|---|---|
| 0.10 | 0.75 | 25.0 |
| 0.10 | 0.75 | 23.0 |
| 0.10 | 0.75 | 28.0 |
| 0.10 | 0.75 | 23.7 |
| 0.10 | 10.0 | 0.21 |
| 0.10 | 10.0 | 0.27 |
| 0.10 | 10.0 | 0.22 |
| 0.10 | 10.0 | 0.23 |
| 0.19 | 10.0 | 0.81 |
| 0.19 | 10.0 | 0.46 |
| 0.19 | 10.0 | 0.29 |
| 0.19 | 10.0 | 0.32 |
| 0.28 | 10.0 | 1.31 |
| 0.28 | 10.0 | 0.22 |
| 0.28 | 10.0 | 1.05 |
| 0.28 | 0.75 | 43.0 |
| 0.28 | 0.75 | 46.0 |
| 0.28 | 0.75 | 48.0 |
| 0.28 | 0.75 | 40.0 |
| 0.97 | 0.75 | 70.0 |
| 0.97 | 1.50 | 37.5 |
| 0.97 | 10.0 | 3.76 |
| 0.97 | 1.50 | 40.0 |
| 0.97 | 2.50 | 24.1 |
| 0.97 | 2.50 | 18.0 |
| 1.95 | 10.0 | 6.6 |
| 1.95 | 10.0 | 6.2 |
| 1.95 | 2.5 | 55.0 |
| 1.95 | 10.0 | 6.8 |

Table 3.9b Peak Blast Pressures Measured Along the 30-Degree Line (Measured from Extended Centerline of the Access Tunnel)

| Loading Density $lb/ft^3$ | Radial Distance ft | Peak Pressure psi |
|---|---|---|
| 0.10 | 3 | 0.91 |
| 0.10 | 3 | 0.75 |
| 0.10 | 5 | 0.82 |
| 0.10 | 5 | 0.65 |
| 0.10 | 8 | 0.63 |
| 0.10 | 8 | 0.68 |
| 0.10 | 8 | 0.30 |
| 0.19 | 3 | 1.7 |
| 0.19 | 3 | 1.9 |
| 0.19 | 5 | 1.4 |
| 0.19 | 5 | 1.57 |
| 0.19 | 8 | 0.70 |
| 0.19 | 8 | 0.69 |
| 0.28 | 3 | 4.35 |
| 0.28 | 3 | 4.9 |
| 0.28 | 5 | 1.5 |
| 0.28 | 5 | 1.5 |
| 0.28 | 8 | 0.85 |
| 0.28 | 8 | 0.78 |
| 0.37 | 3 | 4.8 |
| 0.37 | 3 | 5.8 |
| 0.37 | 5 | 2.38 |
| 0.37 | 5 | 2.4 |
| 0.37 | 8 | 1.6 |
| 0.37 | 8 | 1.59 |
| 0.46 | 3 | 8.4 |
| 0.46 | 5 | 3.6 |
| 0.46 | 8 | 3.0 |

Table 3.9c Peak Blast Pressures Measured Along a 45-Degree Line with Respect to the Extended Center line of the Access Tunnel

| Loading Density $lb/ft^3$ | Radial Distance ft | Peak Pressure psi |
|---|---|---|
| 0.10 | 2.0 | 1.0 |
| 0.10 | 2.0 | 0.9 |
| 0.10 | 3.5 | 1.0 |
| 0.10 | 3.5 | 0.75 |
| 0.10 | 3.5 | 0.64 |
| 0.10 | 7.0 | 0.58 |
| 0.10 | 7.0 | 0.40 |
| 0.10 | 7.0 | 0.40 |
| 0.19 | 2.0 | 1.88 |
| 0.19 | 2.0 | 2.25 |
| 0.19 | 3.5 | 1.9 |
| 0.19 | 3.5 | 2.08 |
| 0.19 | 7.0 | 0.71 |
| 0.19 | 7.0 | 0.69 |
| 0.28 | 2.0 | 8.3 |
| 0.28 | 2.0 | 7.5 |
| 0.28 | 3.5 | 3.0 |
| 0.28 | 3.5 | 2.6 |
| 0.28 | 5.0 | 1.07 |
| 0.28 | 5.0 | 1.08 |
| 0.28 | 7.0 | 0.8 |
| 0.28 | 7.0 | 0.75 |
| 0.37 | 2.0 | 11.2 |
| 0.37 | 2.0 | 7.3 |
| 0.37 | 3.5 | 3.98 |
| 0.37 | 3.5 | 3.85 |
| 0.37 | 5.0 | 1.86 |
| 0.37 | 5.0 | 1.6 |
| 0.37 | 7.0 | 1.56 |
| 0.37 | 7.0 | 1.25 |
| 0.46 | 2.0 | 12.5 |
| 0.46 | 3.5 | 5.3 |
| 0.46 | 5.0 | 3.3 |
| 0.46 | 7.0 | 3.1 |

Table 3.9d Peak Blast Pressures Measured Along the 60-Degree Line (Measured from the Extended Centerline of the Access Tunnel)

| Loading Density $lb/ft^3$ | Radial Distance ft | Peak Pressure psi |
|---|---|---|
| 0.10 | 1.0 | 5.0 |
| 0.10 | 1.0 | 4.25 |
| 0.10 | 2.5 | 0.65 |
| 0.10 | 2.5 | 0.55 |
| 0.10 | 5.0 | 0.70 |
| 0.10 | 5.0 | 0.68 |
| 0.19 | 1.0 | 9.8 |
| 0.19 | 1.0 | 12.5 |
| 0.19 | 2.5 | 1.08 |
| 0.19 | 2.5 | 1.1 |
| 0.19 | 5.0 | 0.92 |
| 0.19 | 5.0 | 0.80 |
| 0.28 | 1.0 | 34.5 |
| 0.28 | 1.0 | 36.5 |
| 0.28 | 2.5 | 3.85 |
| 0.28 | 2.5 | 3.9 |
| 0.28 | 5.0 | 1.0 |
| 0.28 | 5.0 | 1.0 |
| 0.37 | 2.5 | 4.68 |
| 0.37 | 2.5 | 3.7 |
| 0.37 | 5.0 | 1.5 |
| 0.37 | 5.0 | 1.54 |
| 0.46 | 2.5 | 5.25 |
| 0.46 | 5.0 | 2.6 |

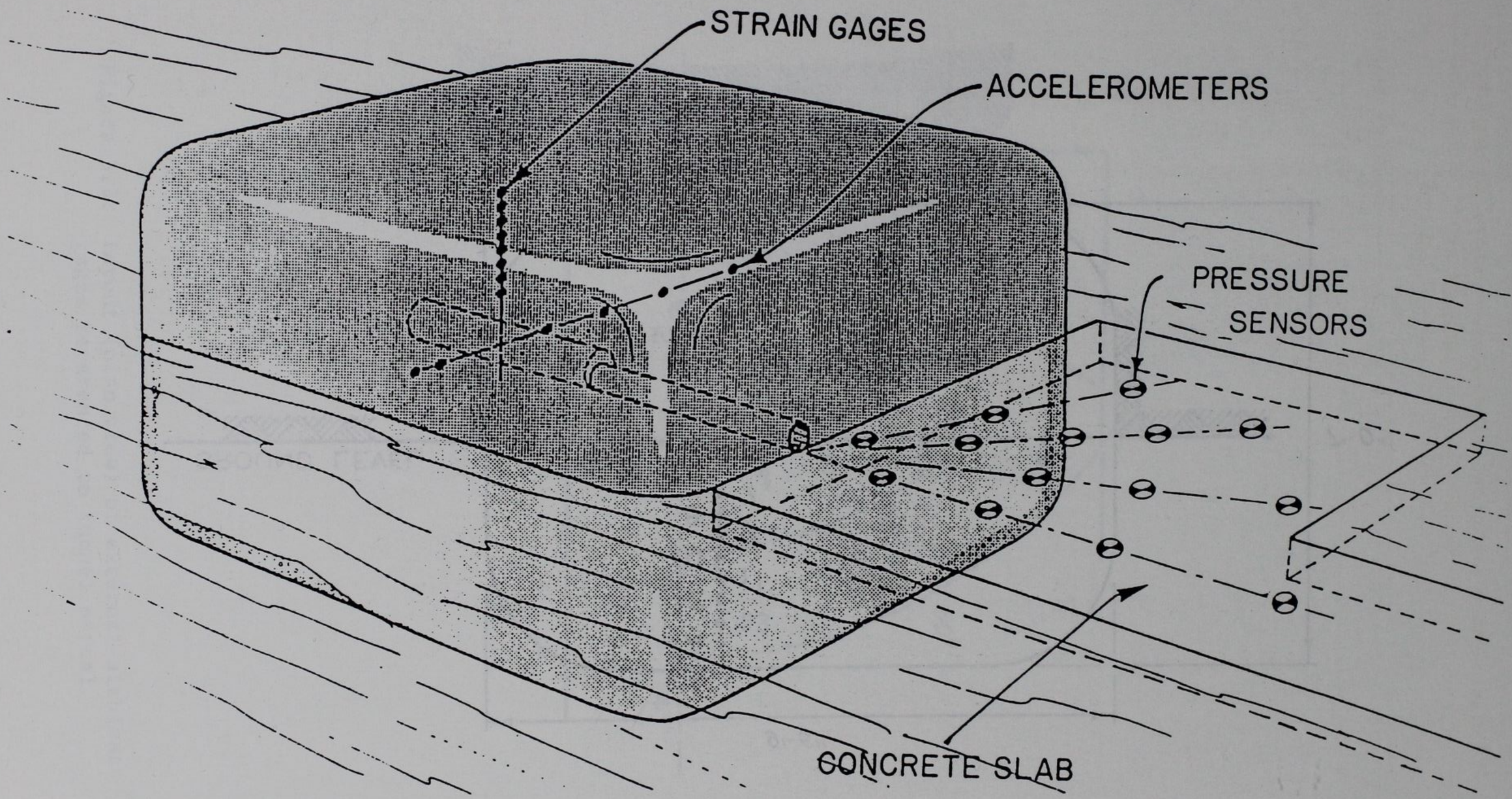


Figure 3.1. Schematic of experimental model.

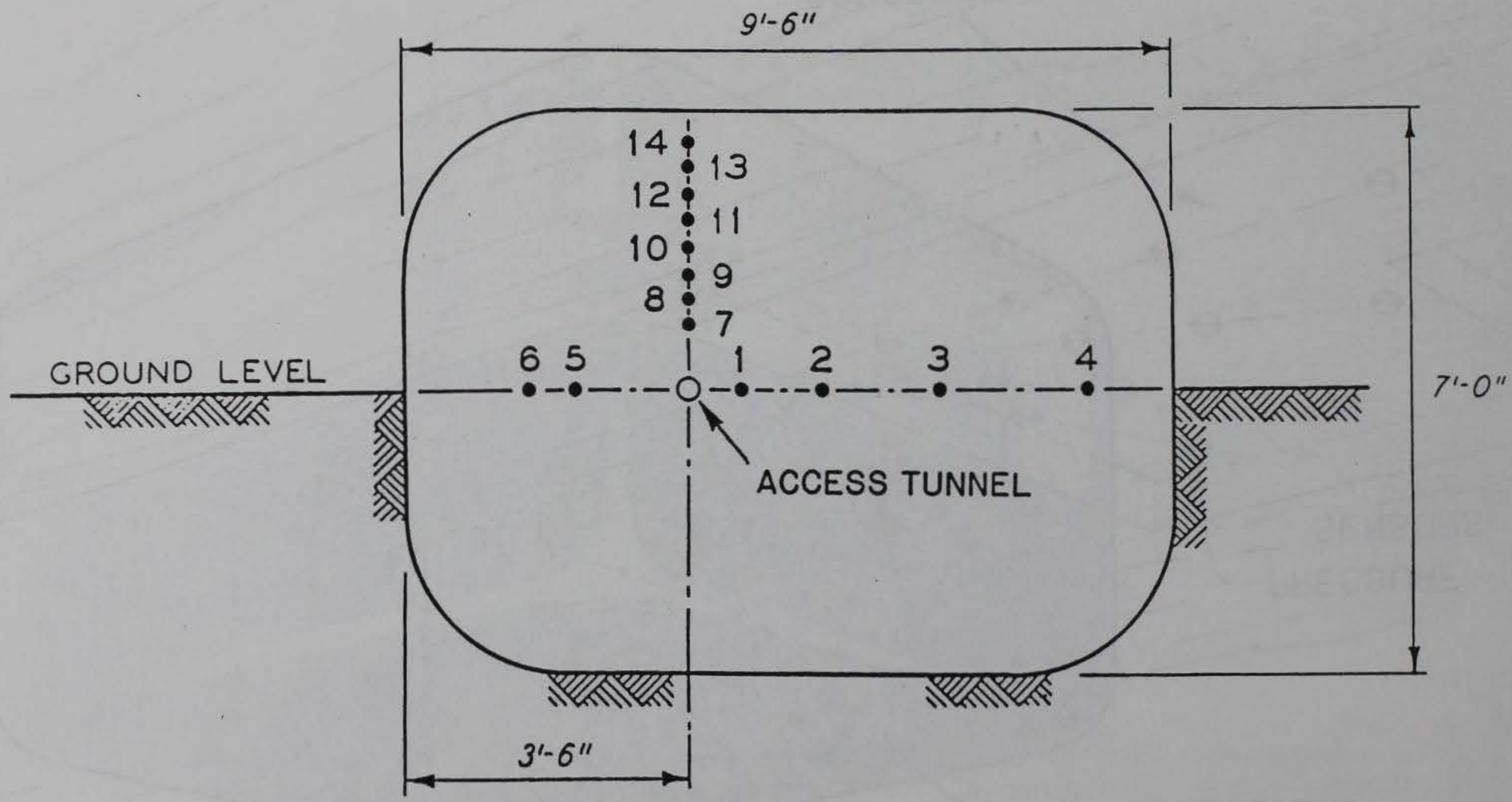


Figure 3.2. Schematic indicating the location of the ground shock gages.

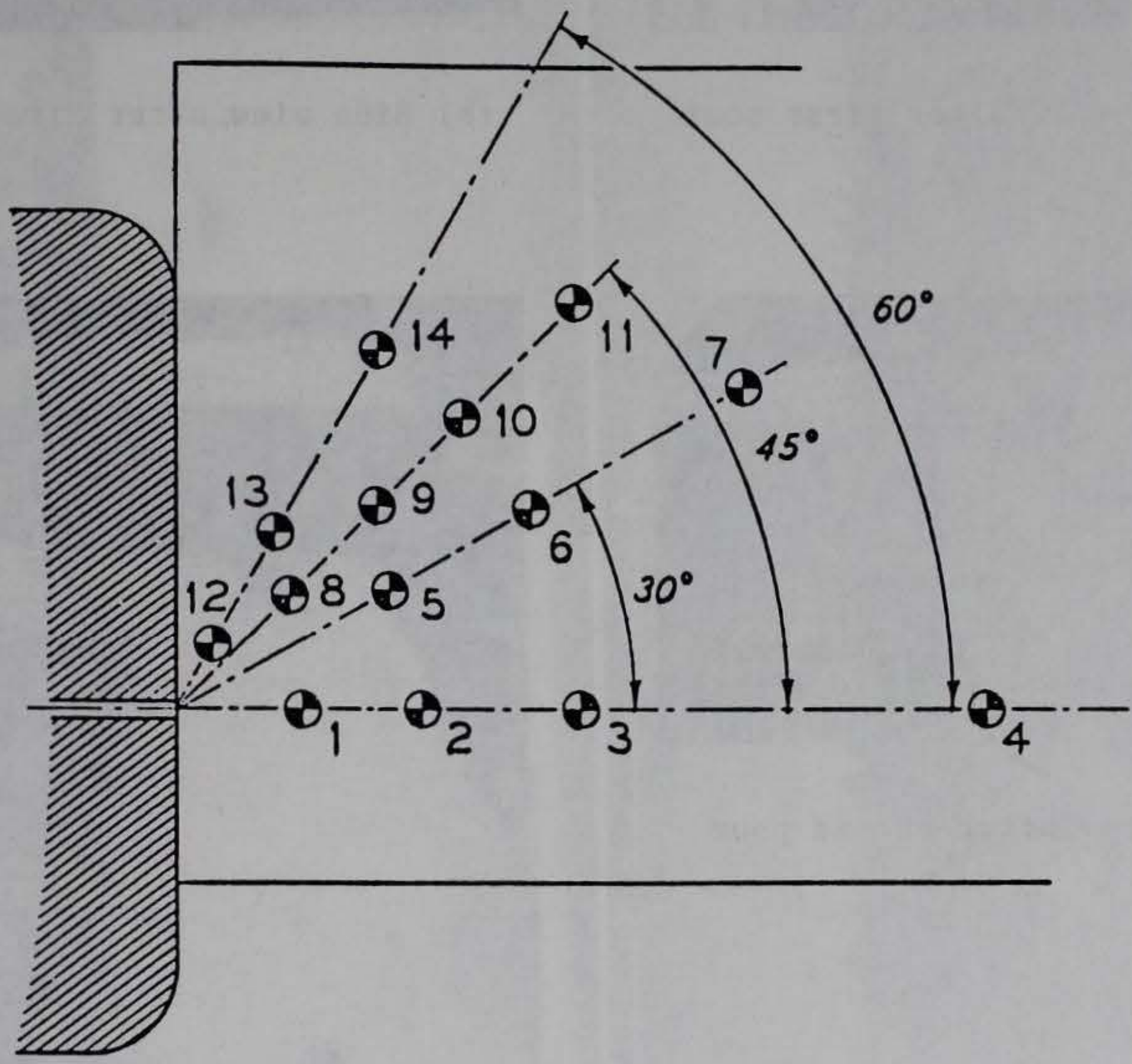


Figure 3.3. Layout (plan view) of external airblast gages referenced to tunnel portal.

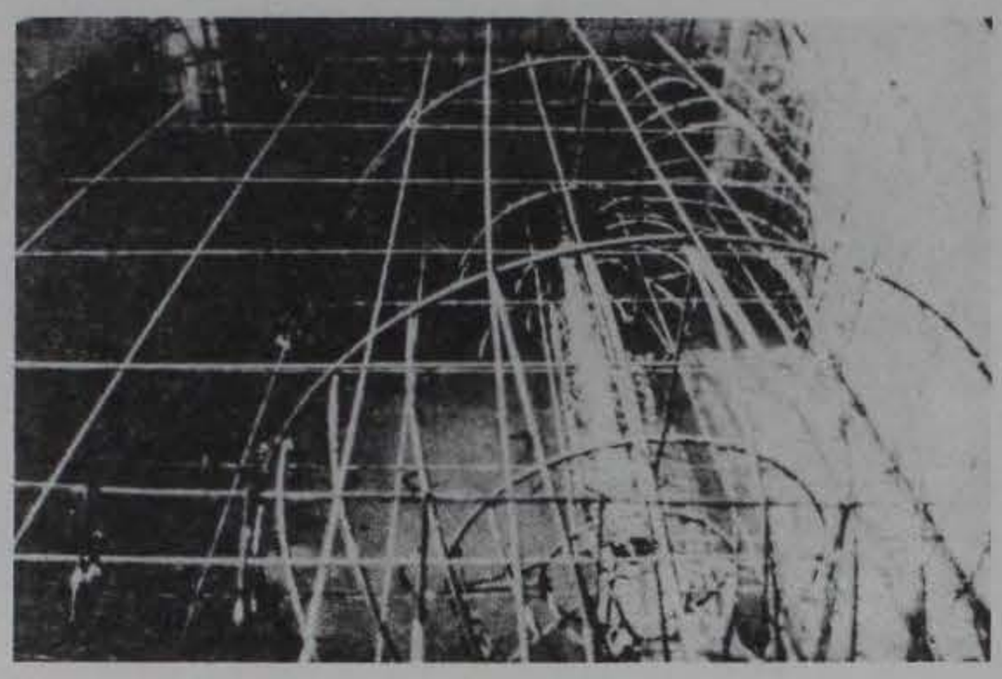

(a) End view after first pour

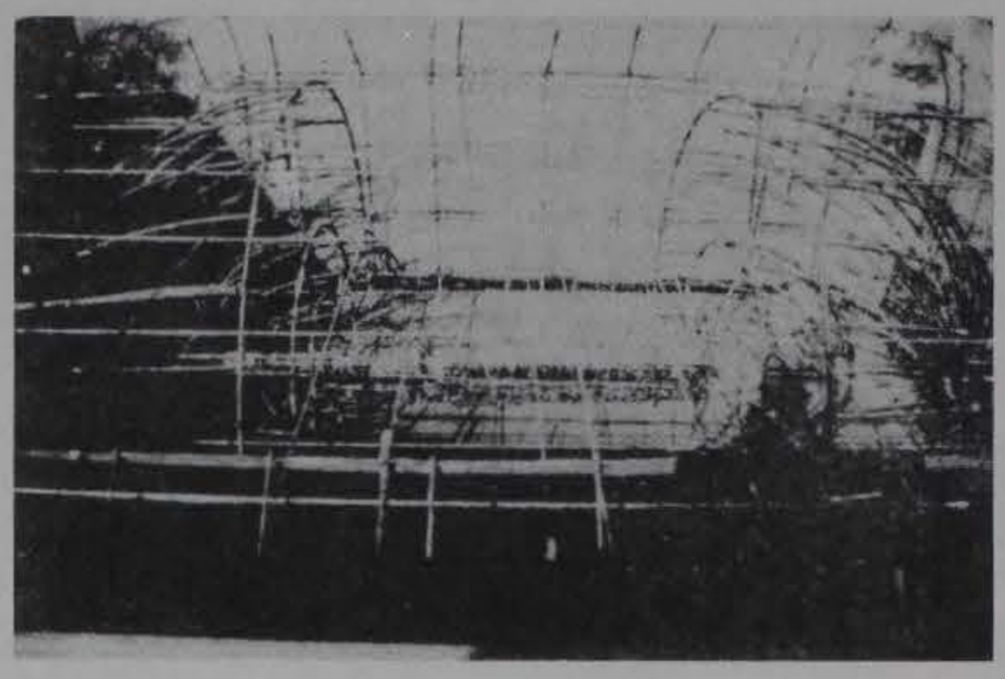

(b) Side view after first pour

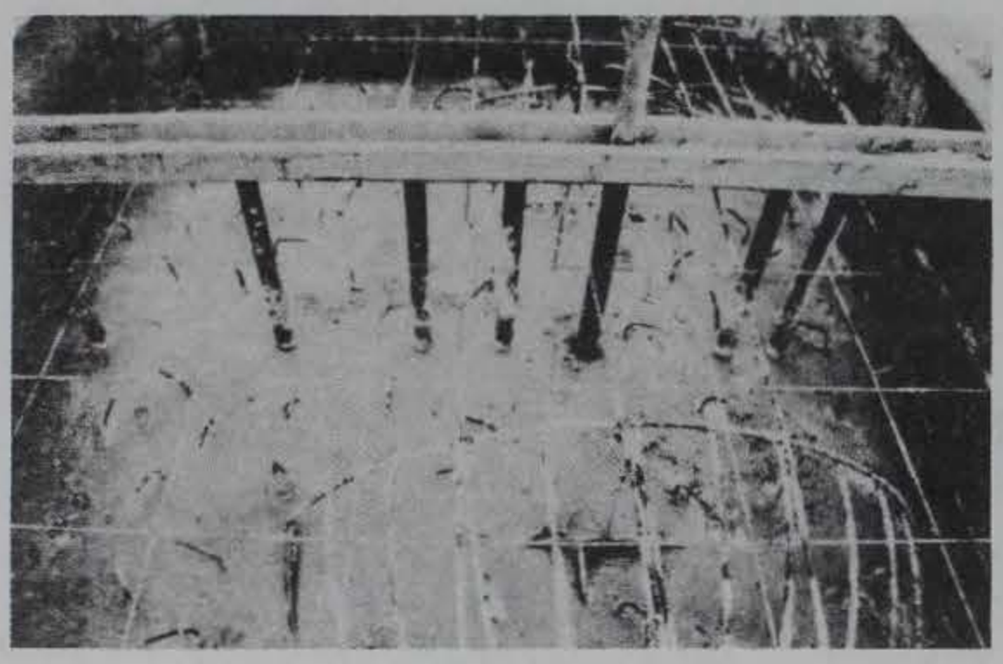

(c) End view after second pour

(d) Completed model

Figure 3.4. Construction of the Small Scale Model.

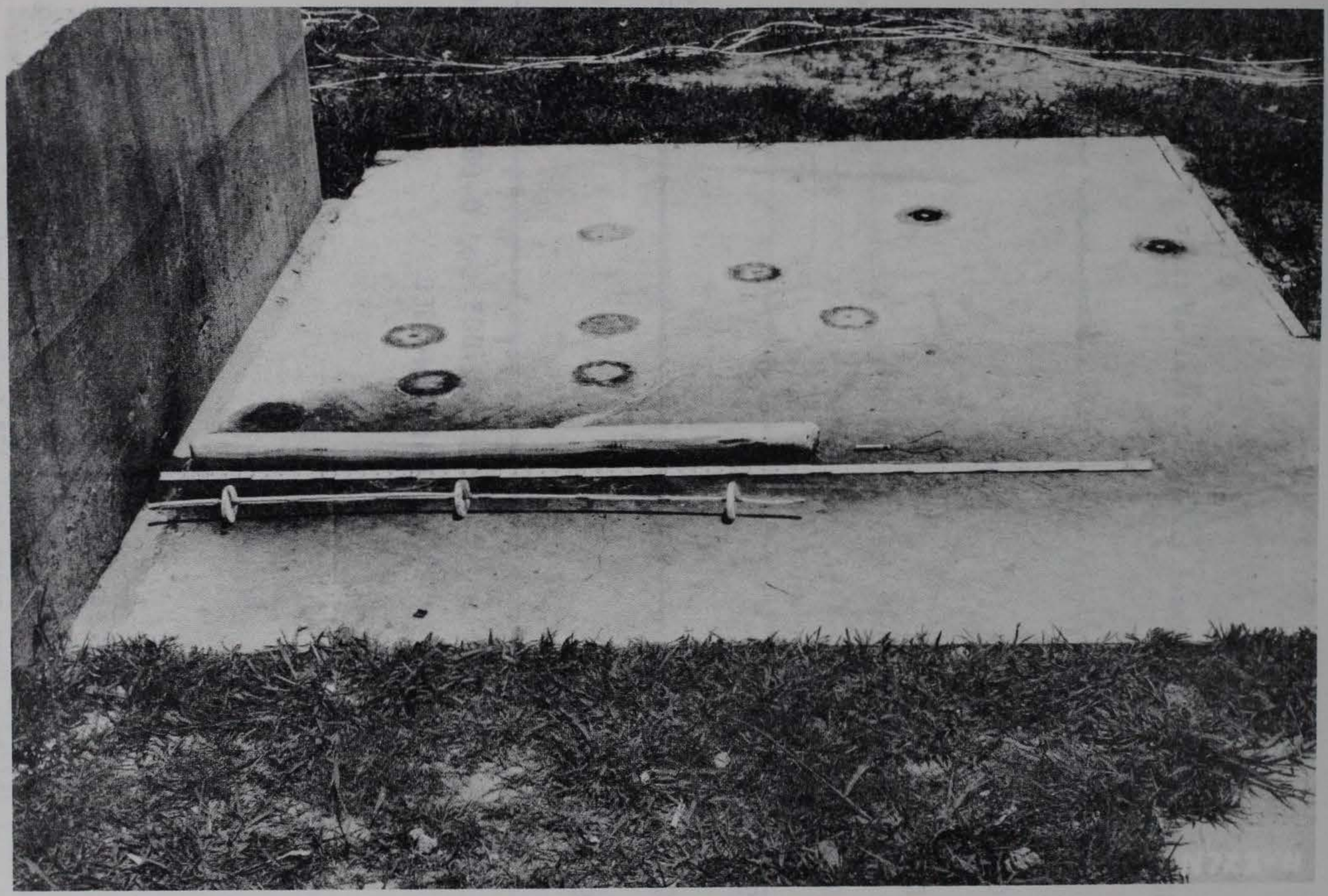

Figure 3.5. The Smallest and Largest Charge Used in the Test Program.

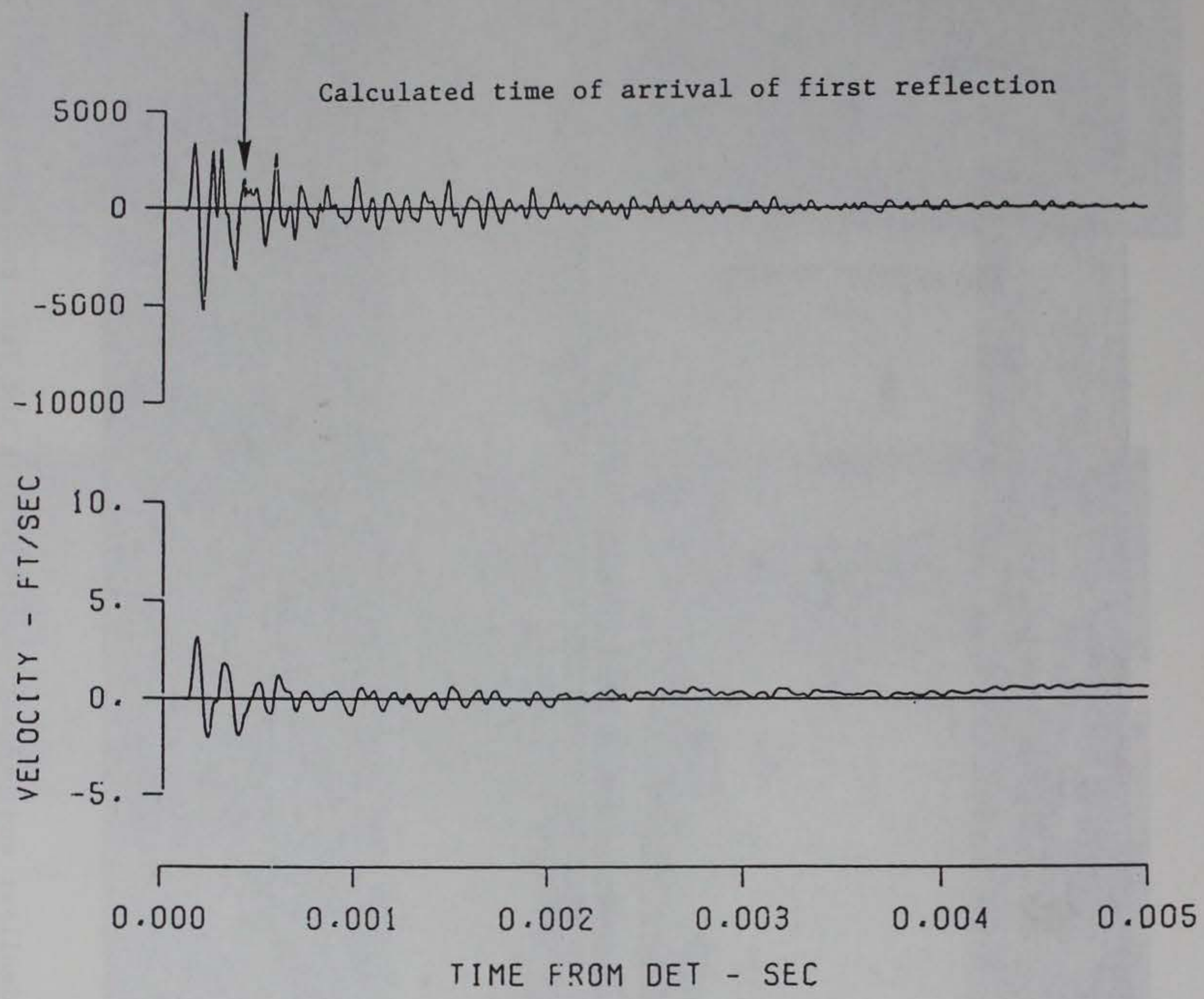


Figure 3.6. Acceleration history obtained at a loading density of 1 $lb/ft^3$. Gage range is 1.378 ft from chamber center line.

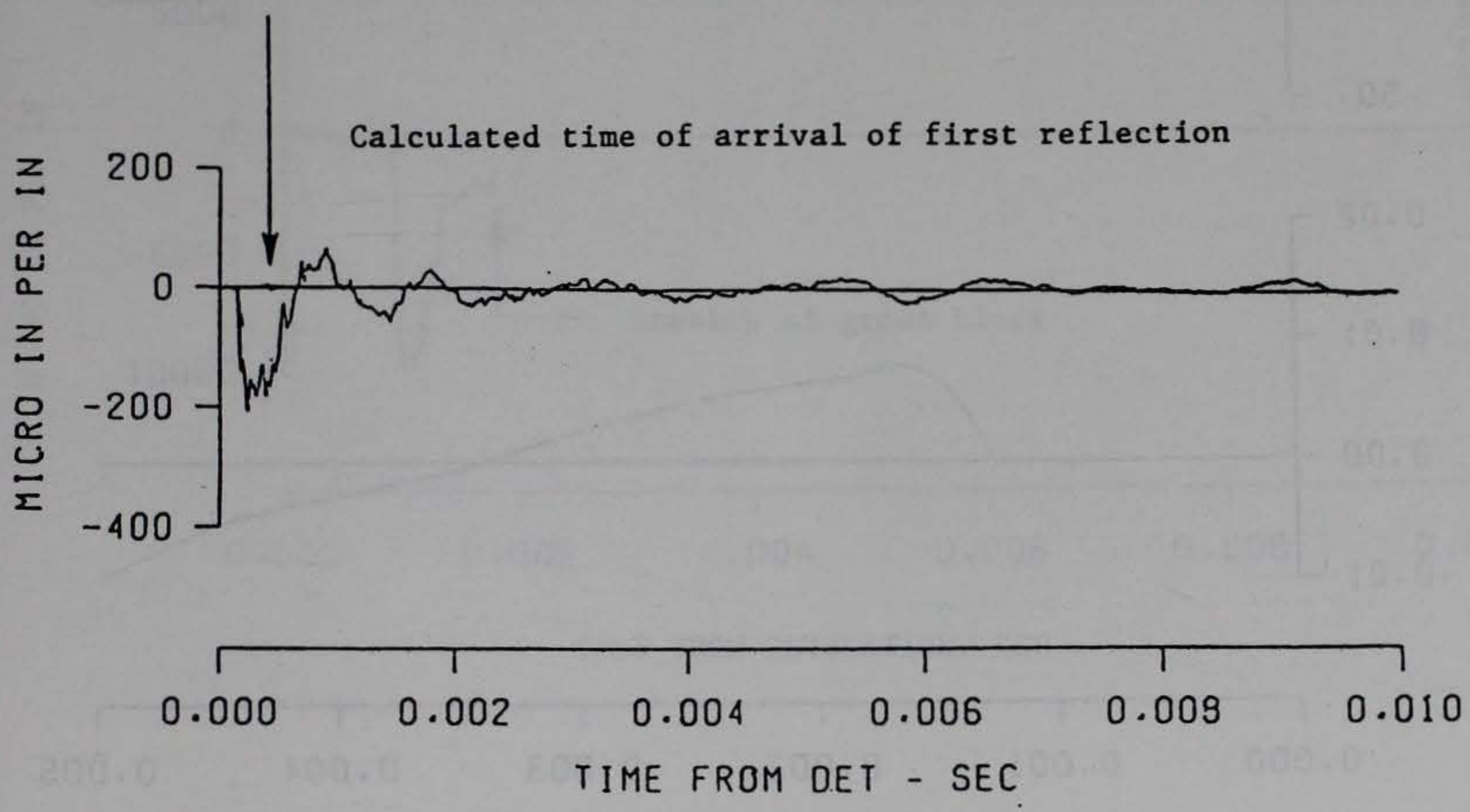


Figure 3.7. Free-field strain measured at a loading density of 1 lb/ft$^3$. Gage range is 1.458 ft from chamber center line.

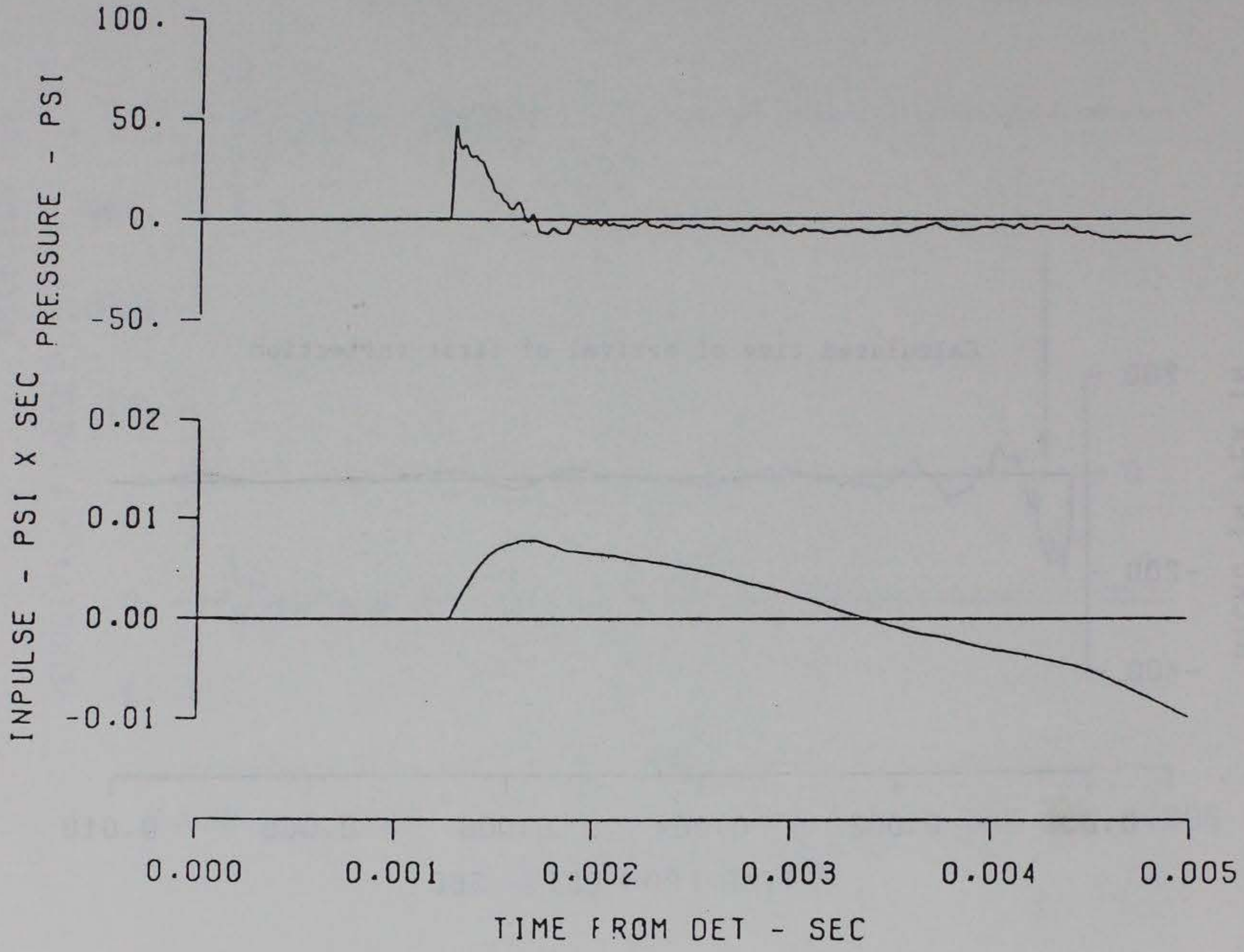


Figure 3.8. Free-field pressure history obtained at a loading density of 2 lb/ft$^3$. Gage on 0-degree line 2.5 ft from tunnel portal.

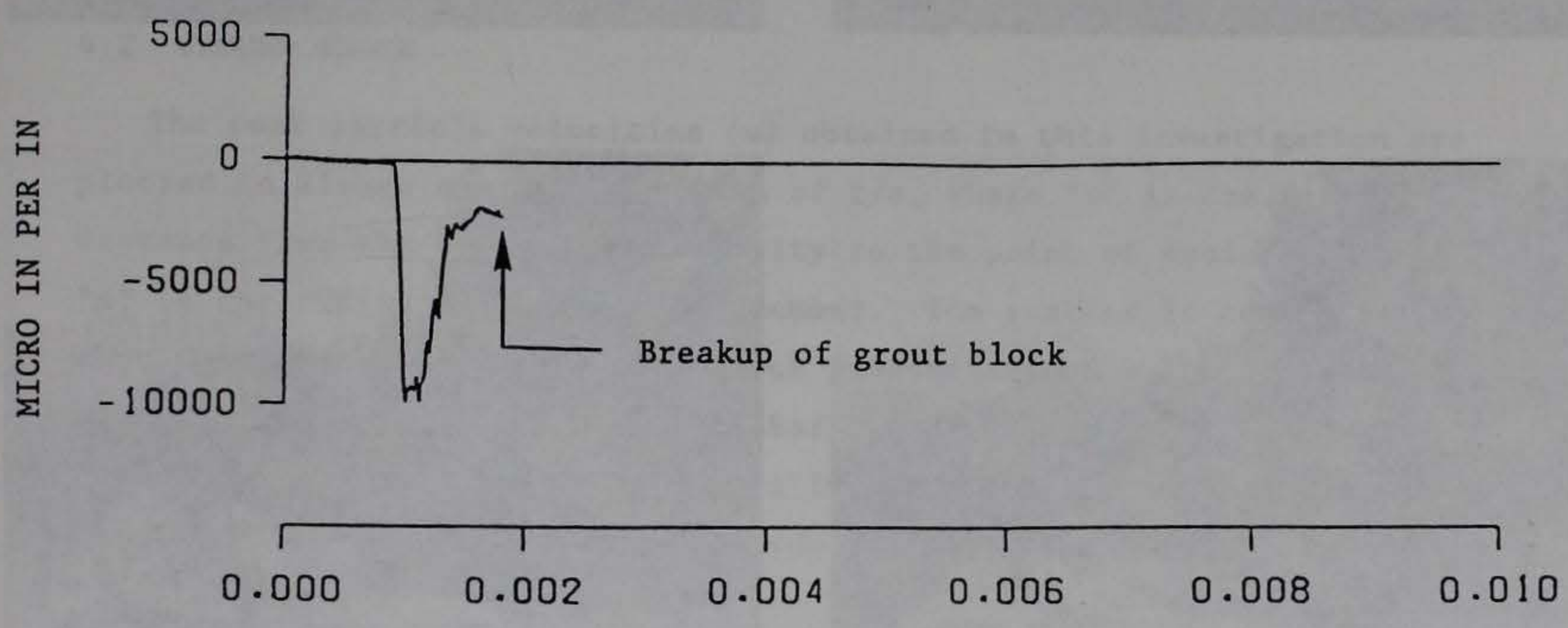


Figure 3.9. Strain history recorded at a loading density of 25.3 lb/ft$^3$. Gage range is 1.458 ft from chamber center line.

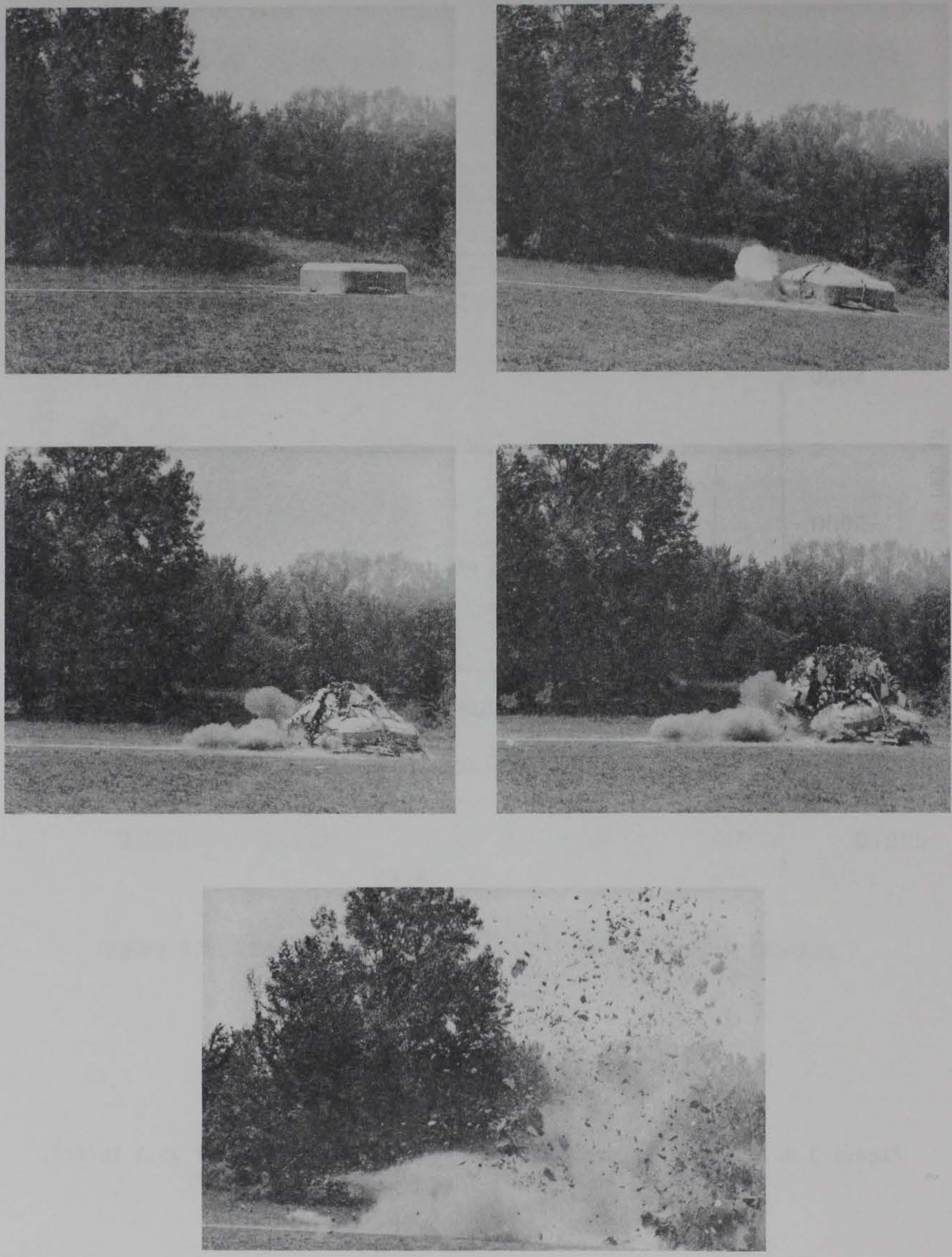

Figure 3.10. Disintegration of the Model with a loading density of 25.25 lb/ft$^3$.

# CHAPTER 4

# ANALYSIS OF DATA

## 4.1 INTRODUCTION

The ground shock and airblast data were analyzed and compared to previously published (through 1978) data. Normalized plots were developed for the ground shock data which identify the point of transition from cylindrical to spherical decay. Dimensionless equations were developed which define the upper bound of the peak free-field strains produced by an explosion in a cylindrical storage chamber of arbitrary size.

## 4.2 GROUND SHOCK

The peak particle velocities (v) obtained in this investigation are plotted in Figure 4.1 as a function of r/a, where "r" is the radial distance from the center of the cavity to the point of measurement and "a" is the radius of the storage chamber. The scatter is consistent with that obtained in typical ground shock investigations. The peak velocity data agrees well with data (Amend, References 21 and 22) obtained from explosions in 2-ft diameter cavities in sandstone and highly-jointed granite. These data represent an order of magnitude increase in cavity diameter, however.

The peak velocity is strongly dependent upon loading density. Comparing the data obtained at 0.1 and 1 $lb/ft^3$, one finds that an order of magnitude increase in loading density results in approximately an order of magnitude increase in peak velocity.

Peak strain data were derived from the peak velocity data by using the approximation

$$\varepsilon = v/c \qquad (4.1)$$

where $\epsilon$ is peak strain

$v$ is peak particle velocity (in./sec)

and $c$ is compressional wave velocity (in./sec)

The peak strains calculated from the peak velocity measurements are compared with the measured peak strains (Table 3.7) in Figures 4.2

through 4.6. To facilitate interpretation, the raw data obtained for each loading density are presented in separate figures. The scatter in the data is consistent with the scatter typically obtained from strain or velocity measurements. It should be noted that the strain measurements were obtained from a vertical array of gages, whereas the velocity data was obtained from a horizontal array. Agreement of the data demonstrates that there were no apparent directional anomalies.

The data obtained near the chamber is consistent with previously published results obtained at radial distances equal to several cavity lengths (Atchison, Reference 19). This is indicated in Figure 4.6 by comparing the data at the 25.3 $lb/ft^3$ loading with Atchison's data obtained at 21.6 $lb/ft^3$.

As demonstrated by Drake (Reference 20), Atchison's data is dominated by spherical decay. As indicated in Figure 4.6, the slope of the data obtained in this investigation appears to asymptotically approach a spherical decay, although the precise point of transition from cylindrical to spherical decay cannot be clearly ascertained. It can, however, be determined from a normalized plot as a result of an increase in data density.

The strain at the cavity wall is determined essentially by the chamber pressure and the properties of the medium. As a first approximation, the strain at the wall is given by

$$\varepsilon_w = P_o/E_o \qquad (4.2)$$

where $\epsilon_w$ is the strain at the wall

$P_o$ is the chamber pressure (psi)

and $E_o$ is the elastic modulus of the medium (psi)

The chamber pressure is determined by the loading density and the chemical composition of the explosive. It may be determined for PETN from Figure 2.2. Since the strain at the wall is the maximum strain, Equation 4.2 may be employed to normalize the preceding strain data.

The normalized data presented in Figure 4.7 contains strain data for loading densities encompassing over two orders of magnitude (0.1 to

25.3 lb/ft$^3$). The data coalesces with no increase in data scatter. Excellent agreement exists between the data obtained in this investigation and both the near-field data reported by Amend (References 21 and 22) and the far-field data reported by Atchison, et al. (Reference 19).

The transition from cylindrical to spherical decay occurs at a value of r/a approximately equal to 11.8, which corresponds to a radial distance equal to one-half the length of the cavity. The rate of decay of peak strain in the cylindrical region where $\frac{r}{a} < \frac{L}{2a}$, and in the spherical region, where $\frac{r}{a} > \frac{L}{2a}$, is $r^{-1/2}$ and $r^{-2}$, respectively. Although the cylindrical decay region is apparent, data were not obtained in this investigation at radial distances less than L/4 (or r/a < 5). The data reported by Amend for $\frac{r}{a} = 3$ are included. The line which appears to best fit the data in the cylindrical decay region is extrapolated to the cavity wall (r/a = 1) in Figure 4.7. The theoretical intercept should be 1.0 compared to the suggested value of 1.2. Considering the range of loading densities investigated, inelastic effects near the cavity surface, and the scatter inherent in strain data, the experimentally implied intercept agrees remarkably well with theory.

Lines which identify the upper bound of the data obtained from this particular geometry are indicated in Figure 4.7. Employing the above results, the upper bound of the peak free-field strain produced by an explosion in an arbitrary cylindrical cavity can be determined. It has been established in this investigation that the transition from cylindrical to spherical decay will occur at radial distances on the order of one-half the cavity length. The slopes in the respective region have been demonstrated in this and several other investigations. Additionally, the upper bound of the normalized strain intercept was determined to be 2.4. Using these results, the upper bound equations were found to be

$$\varepsilon E_o/P_o = 2.4(r/a)^{-1/2}; \text{ when } r/a < L/2a \qquad (4.3a)$$

and

$$\varepsilon E_o/P_o = 0.85(L/a)^{1.5}(r/a)^{-2}; \text{ when } r/a > L/2a \qquad (4.3b)$$

For larger standoff distances, a more convenient equation is desirable. From Figure 2.1, it can be observed that the chamber pressure generated by a TNT explosion varies nearly linearly with loading density for loading densities between 0.1 and 25.3 $lb/ft^3$. As a result, the chamber pressure can be closely approximated by

$$P_o = 2580\ (\gamma)^{0.981}$$

where $P_o$ is the chamber pressure (psi) and $\gamma$ is the TNT-equivalent loading density ($lb/ft^3$). However, to simplify the equation which will be developed and to increase conservatism, an exponent of unity is assumed.

Substituting for $P_o$ and rearranging Equation 4.3 we obtain

$$r/a = 3.83 \times 10^7(\gamma/\varepsilon E_o)^2; \text{ when } r/a \quad L/2a \qquad (4.4a)$$

and

$$r/a = 46.8(L/a)^{0.75}(\gamma/\varepsilon E_o)^{1/2}; \text{ when } r/a \quad L/2a \qquad (4.4b)$$

Equation 4.4 is employed in the next chapter to predict the safe standoff distances required for ground shock. Since the equation predicts the maximum distance at which a specified strain will occur, the predicted standoff distances will be safely conservative.

## 4.3 AIRBLAST

The peak free-field airblast data obtained in this investigation are tabulated in Table 3.8. These data are presented in Figures 4.8 through 4.11 as a function of the exit pressure ($P_E$), diameter of the access tunnel (D), and range (r). The exit pressure at the portal was determined from Equation 2.1. The nondimensionalized peak free-field blast data obtained along the extended centerline and the 30, 45 and 60-degree lines (with the 0-degree line being the extended centerline) are presented in Figures 4.8 through 4.11, respectively. Data obtained by other investigators are also included and upper bound curves are indicated.

Data obtained along the extended centerline (Figure 4.2) with loading densities of 0.97 and 1.95 lb/ft$^3$ agree with data obtained by other investigators (Skjeltorp, References 4 and 10) for exit geometries with 0 and 30-degree surface slopes. This result indicates that the standoff distance required along the extended centerline is not sensitive to exit slopes between 0 and 30 degrees. At low loading densities (0.1, 0.19 and 0.28 lb/ft$^3$), the data obtained at large scaled distances (r/D = 44.8) had substantial scatter. This scatter does not appear to be geometrically dependent, however.

Substantial data scatter exists in all of the data obtained along the 30, 45 and 60-degree lines (Figures 4.9, 4.10 and 4.11). It is the author's opinion that this occurred because these experiments were conducted with low loading densities (0.1 to 0.46 lb/ft$^3$) to prevent damage to the model prior to completion of the ground shock investigations. As discussed earlier, low-strength shocks produced by low loading densities appear to be substantially attenuated by microscopic wall roughness. This results in lower exit pressures than predicted and, consequently, a reduced level of shock propagates outside the portal. These effects are nonlinearly related to the loading density. Since the loading density is used to calculate the exit pressure, data scatter results. Gurke and Scheklinski (Reference 15) reported similar results at low loading densities.

Based upon the data presented in Figures 4.8 through 4.11, the upper bound of the free-field blast pressure can be expressed in the dimensionless form:

$$P/P_E = C_\Theta (R/D)^{-3/2} \qquad (4.5)$$

where R is the radial distance from the portal (ft)

D is the effective diameter of the access tunnel (ft)

P is the peak blast pressure (psi) at R

$P_E$ is the peak overpressure at the tunnel exit (psi)

and $C_\Theta$ is a directional coefficient dependent upon the direction of measurement with respect to the extended center line.

The values of $C_\Theta$ as a function of $\Theta$ are:

| $\Theta$: | $0^\circ$ | $30^\circ$ | $45^\circ$ | $60^\circ$ |
|---|---|---|---|---|
| $C_\Theta$: | 3.8 | 3.2 | 3.2 | 2.0 |

Equation 4.5 is consistent with Equation 2.3 developed by Skjeltorp (Reference 4). The dimensionless form of Equation 4.5 provides a method for predicting the standoff distance required as a function of a blast pressure threshold for structures in the particular area of interest, or as a function of different peak pressure criteria used in various countries.

In all directions from the portal, the upper bound of the airblast data obtained in this investigation is consistent with the results obtained by other investigators. Also, the rate of peak pressure decay is consistent with Westine's (Reference 16) gun blast data and the free-field blast data obtained by other investigators.

## 4.4 SUMMARY

Equations have been developed which predict the upper bound of the free-field strain produced by decoupled explosions in cylindrical cavities of finite length, sited in competent rock. Cylindrical wave propagation was found to be dominant out to a maximum radial distance (from the center of the cavity) equal to one-half of the cavity length. At larger radial distances, the peak free-field parameters will be dominated by spherical wave propagation. These results may be used to determine safe standoff distances related to ground shock effects. The upper bound of the airblast data obtained in this investigation was consistent with that found by other investigators.

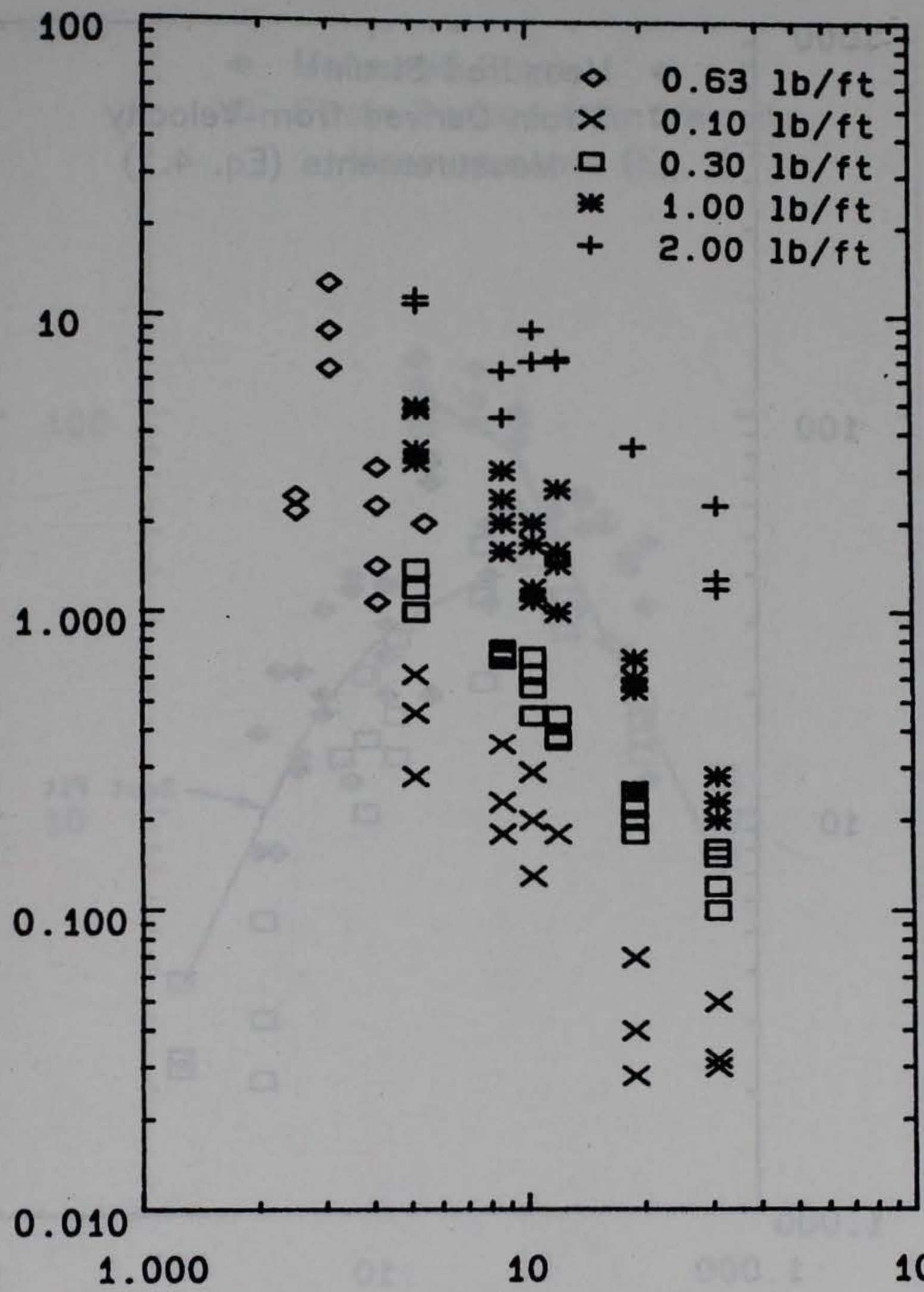


Figure 4.1. Peak particle velocity versus dimensionless distance (distance "R" divided by chamber radius "A") from the center of cavity.

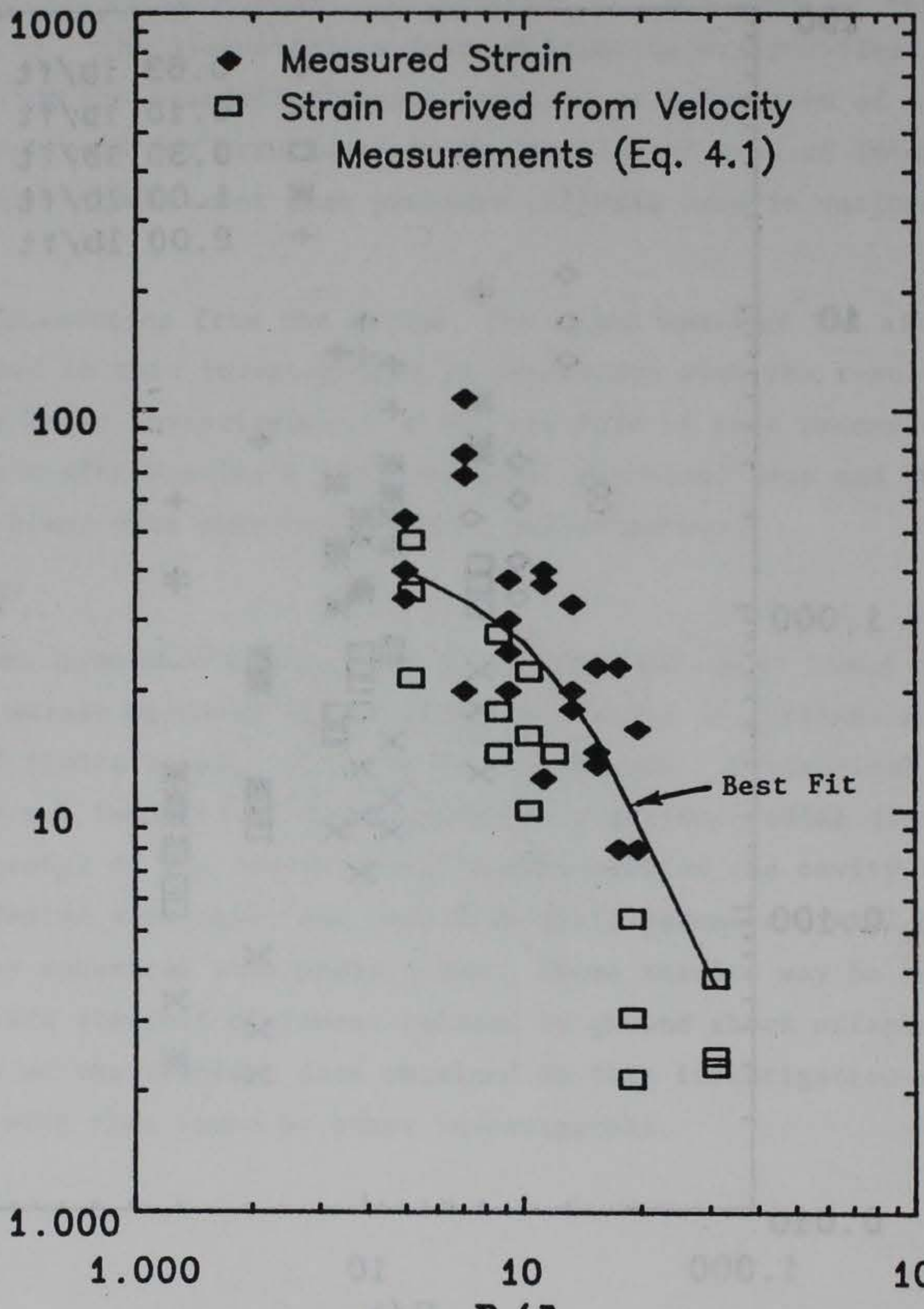


Figure 4.2. Peak strain as a function of dimensionless distance (distance "R" divided by chamber radius "A") obtained at a loading density of 0.1 lb/ft$^3$.

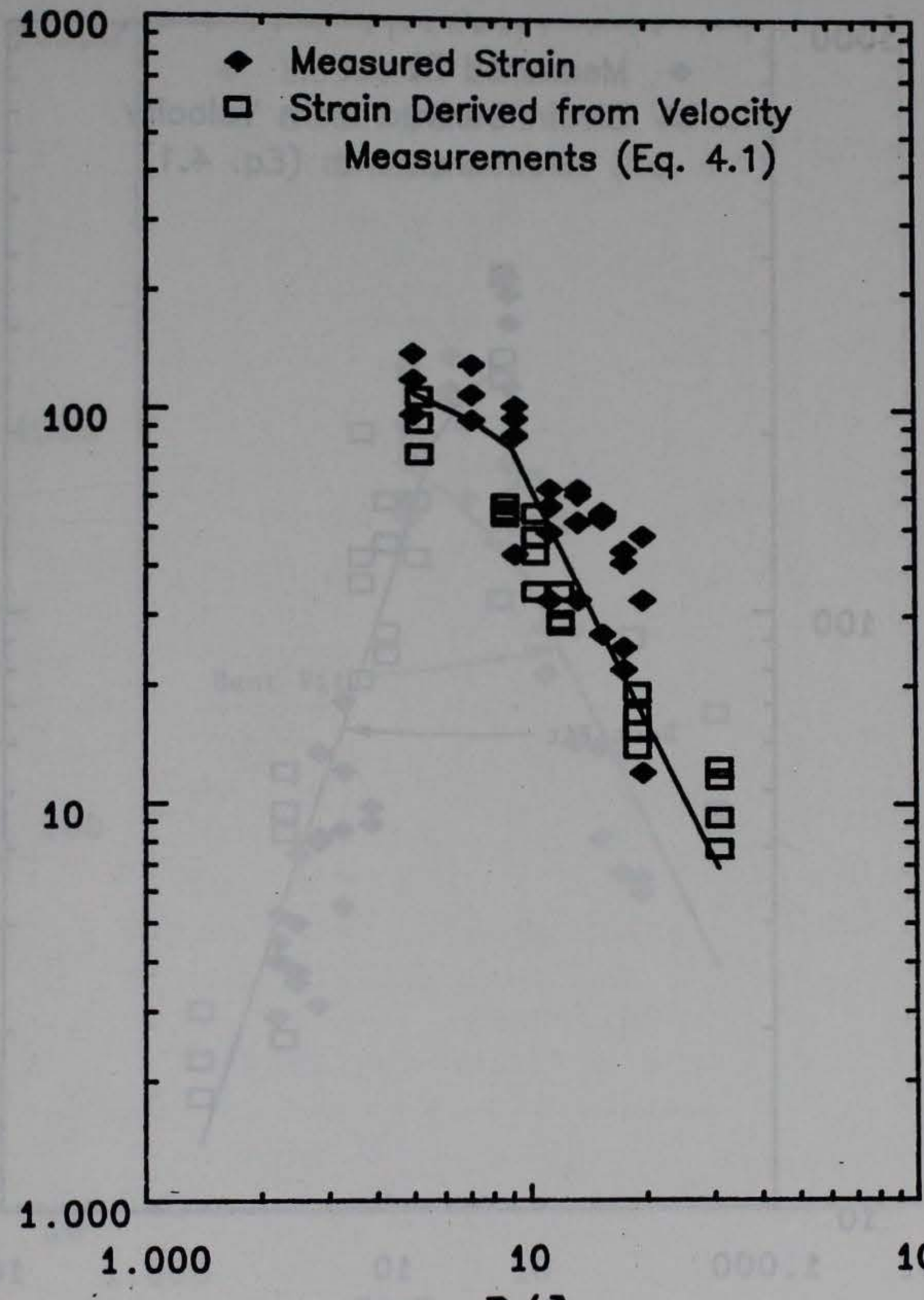


Figure 4.3. Peak strain as a function of dimensionless distance (distance "R" divided by chamber radius "A") obtained at a loading density of 0.3 lb/ft$^3$.

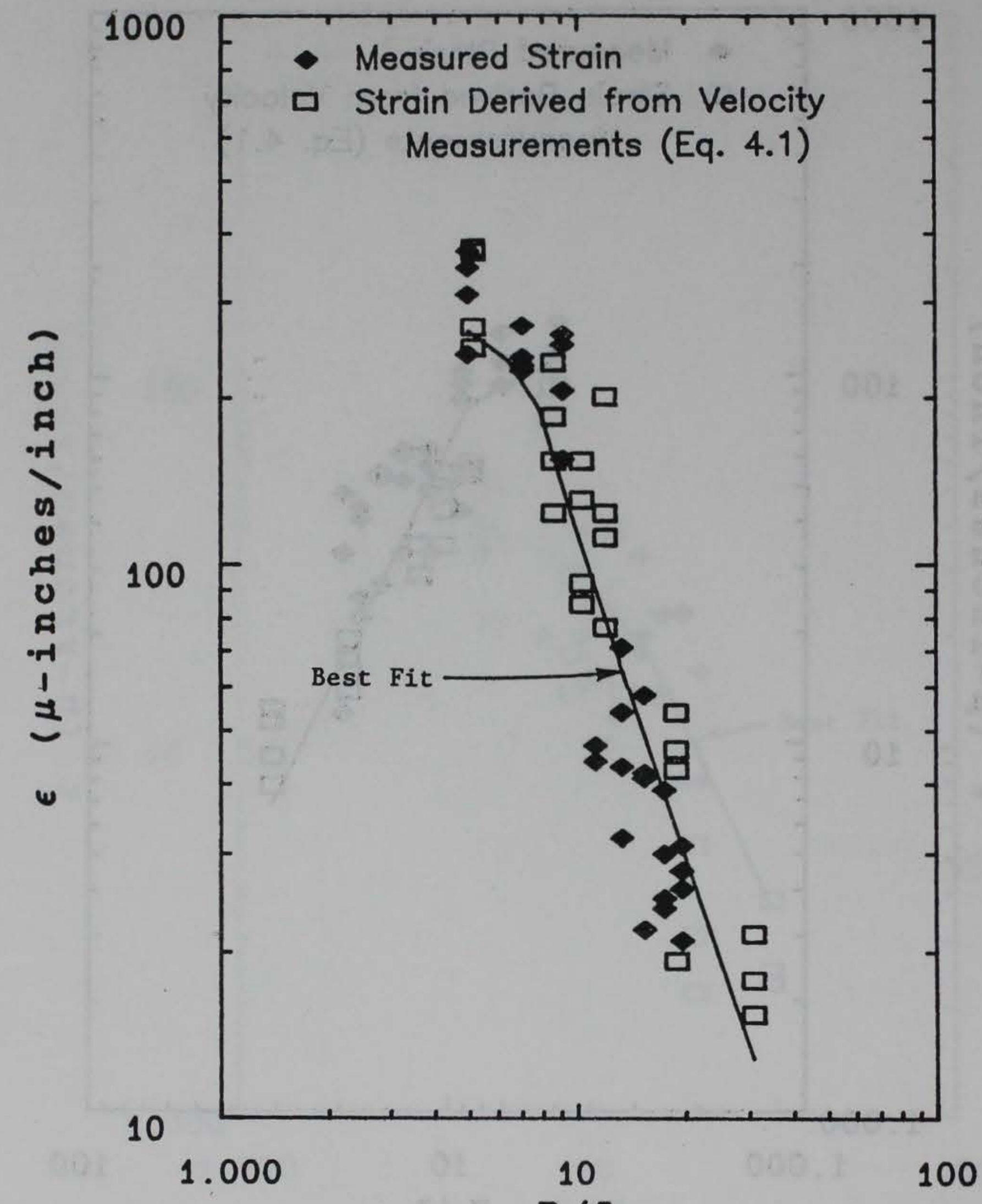


Figure 4.4. Peak strain as a function of dimensionless distance (distance "R" divided by chamber radius "A") obtained at a loading density of 1.0 lb/ft$^3$.

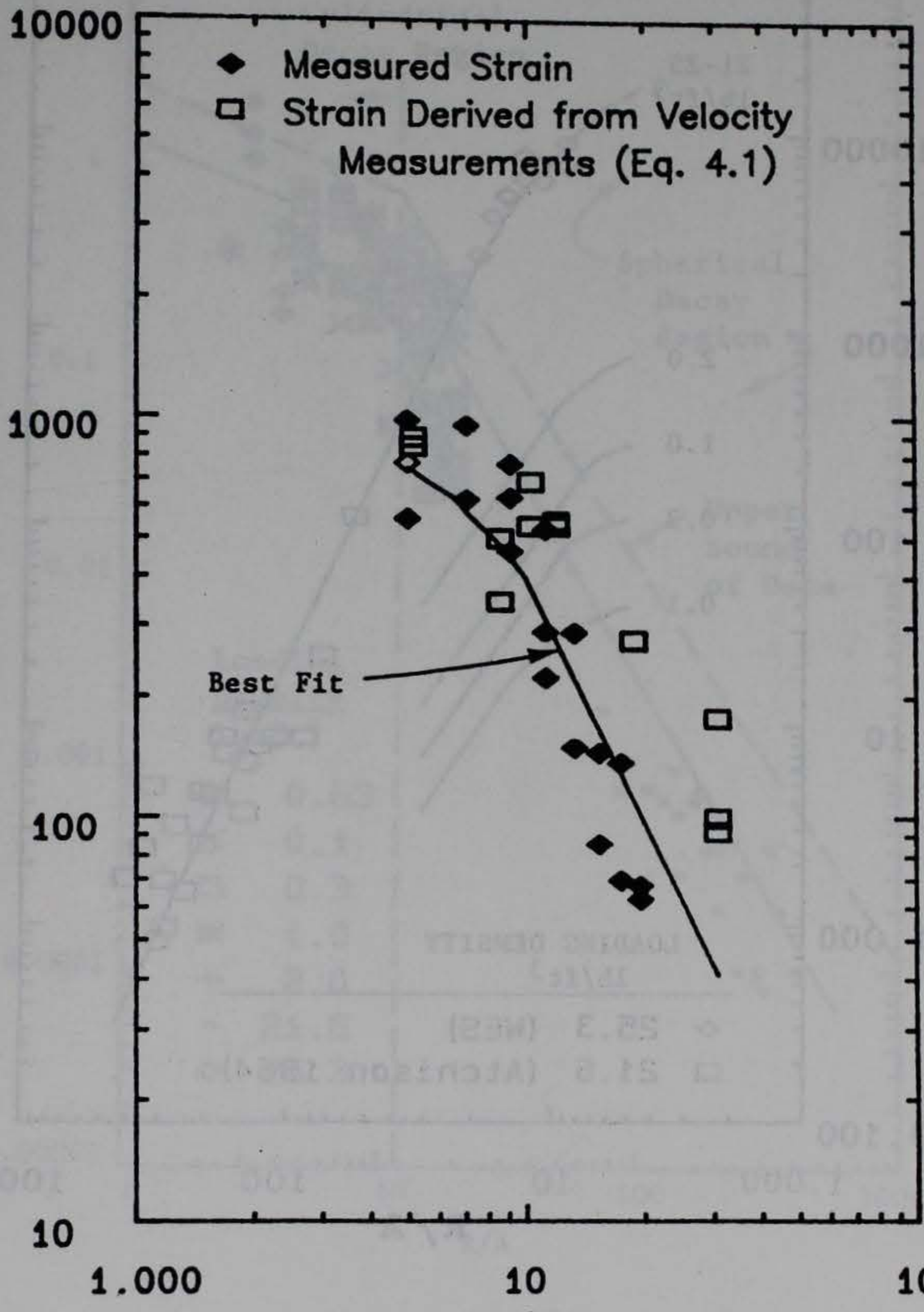


Figure 4.5. Peak strain as a function of dimensionless distance (distance "R" divided by chamber radius "A") obtained at a loading density of 2.0 lb/ft$^3$.

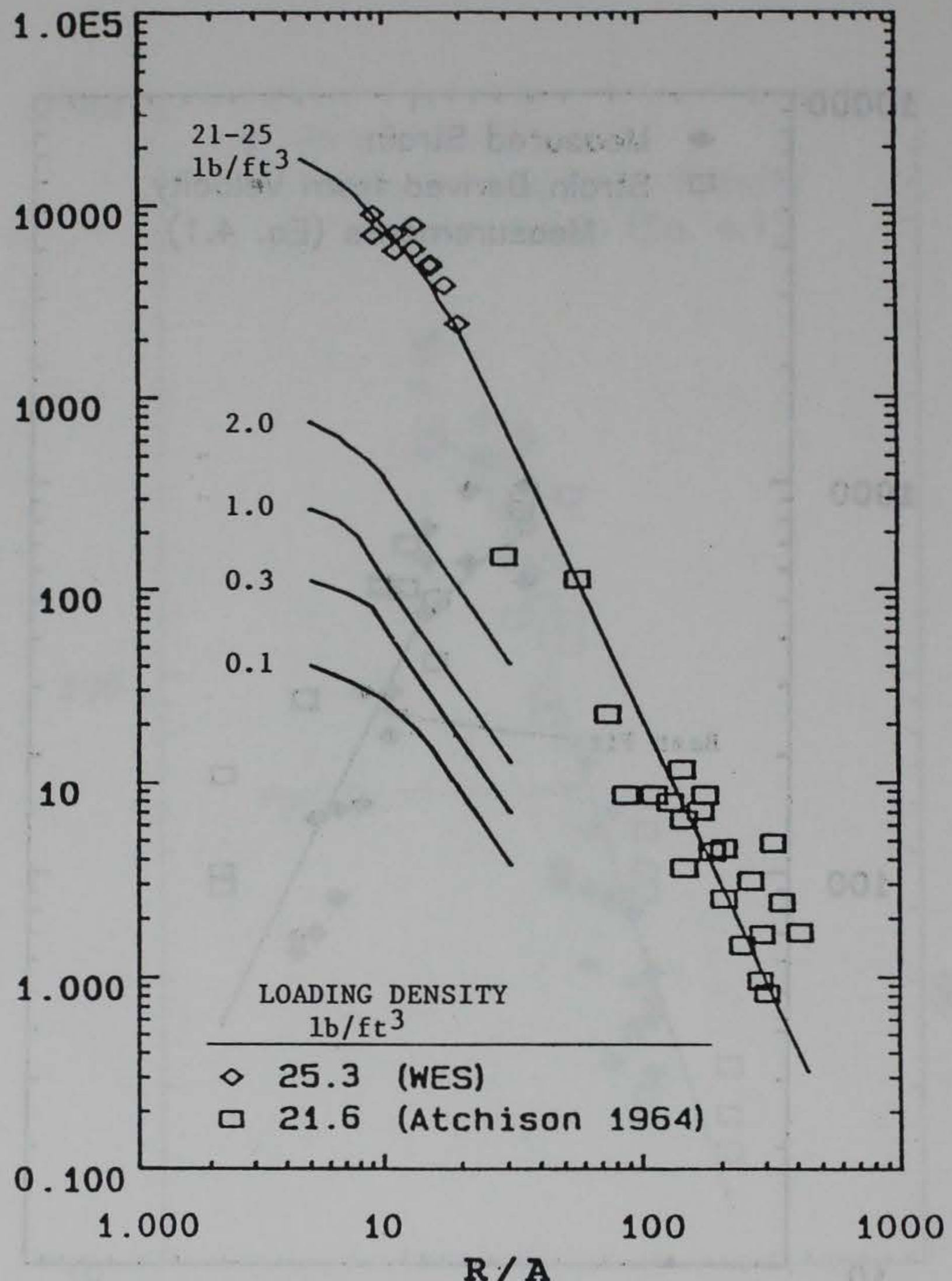


Figure 4.6. Peak strain as a function of dimensionless distance (distance "R" divided by chamber radius "A") for loading densities ranging from 0.1 to 25.3 lb/ft$^3$.

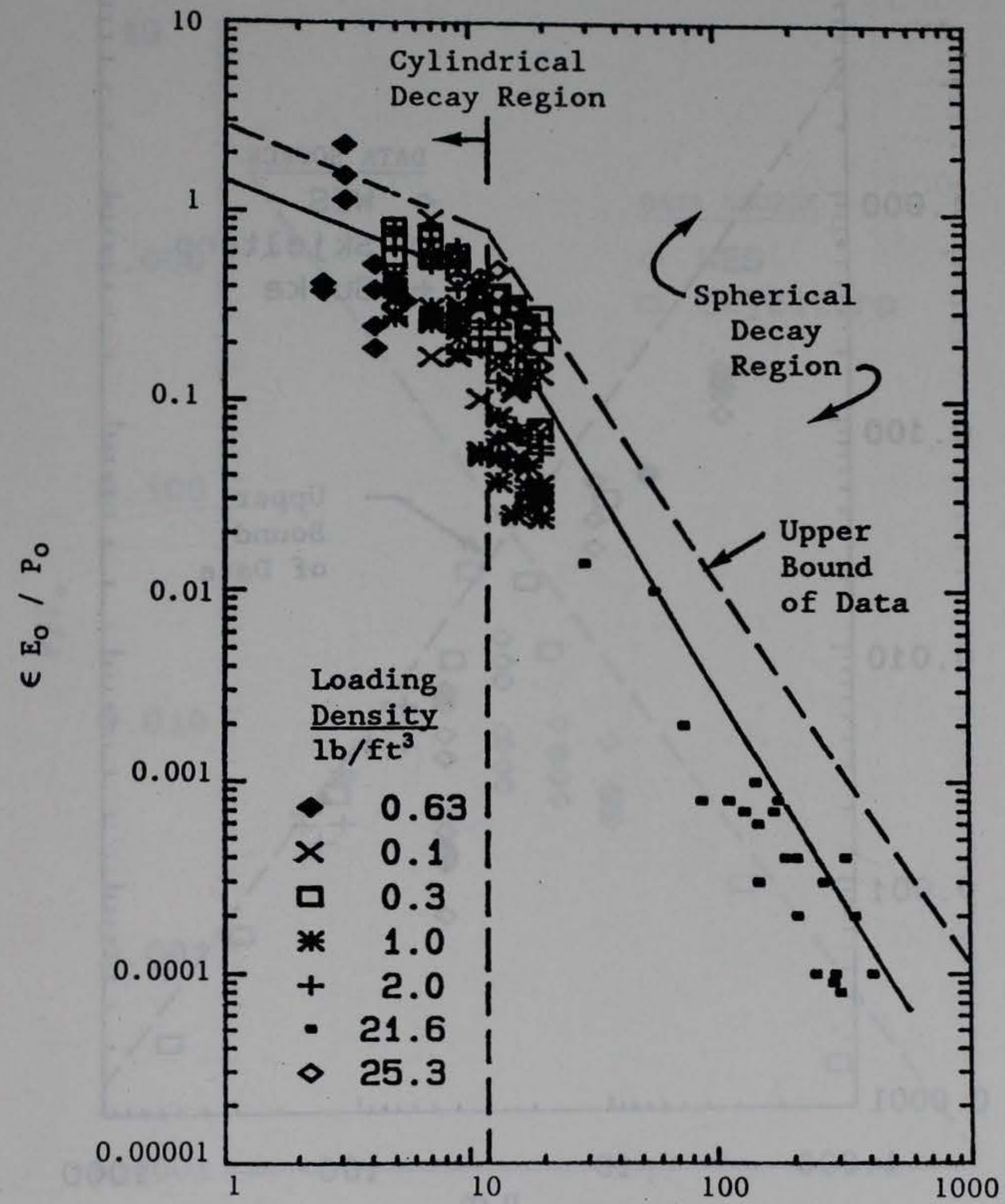


Figure 4.7. Normalized strain as a function of dimensionless distance (distance "R" divided by chamber radius "A").

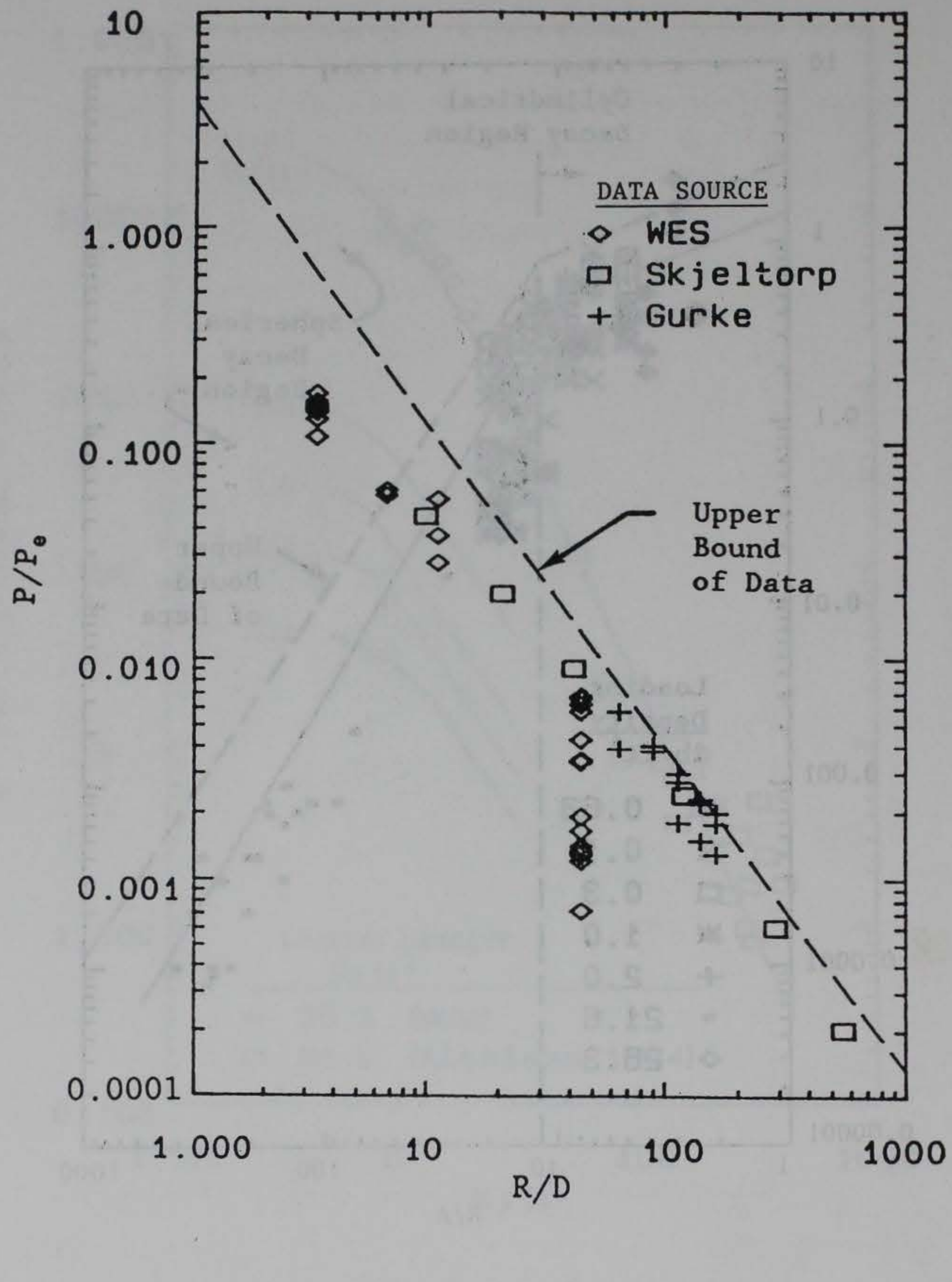


Figure 4.8. Normalized blast data (measured peak pressure "P" divided by chamber pressure "$P_e$") along the extended centerline as a function of dimensionless distance (distance "R" divided by the access tunnel diameter "D").

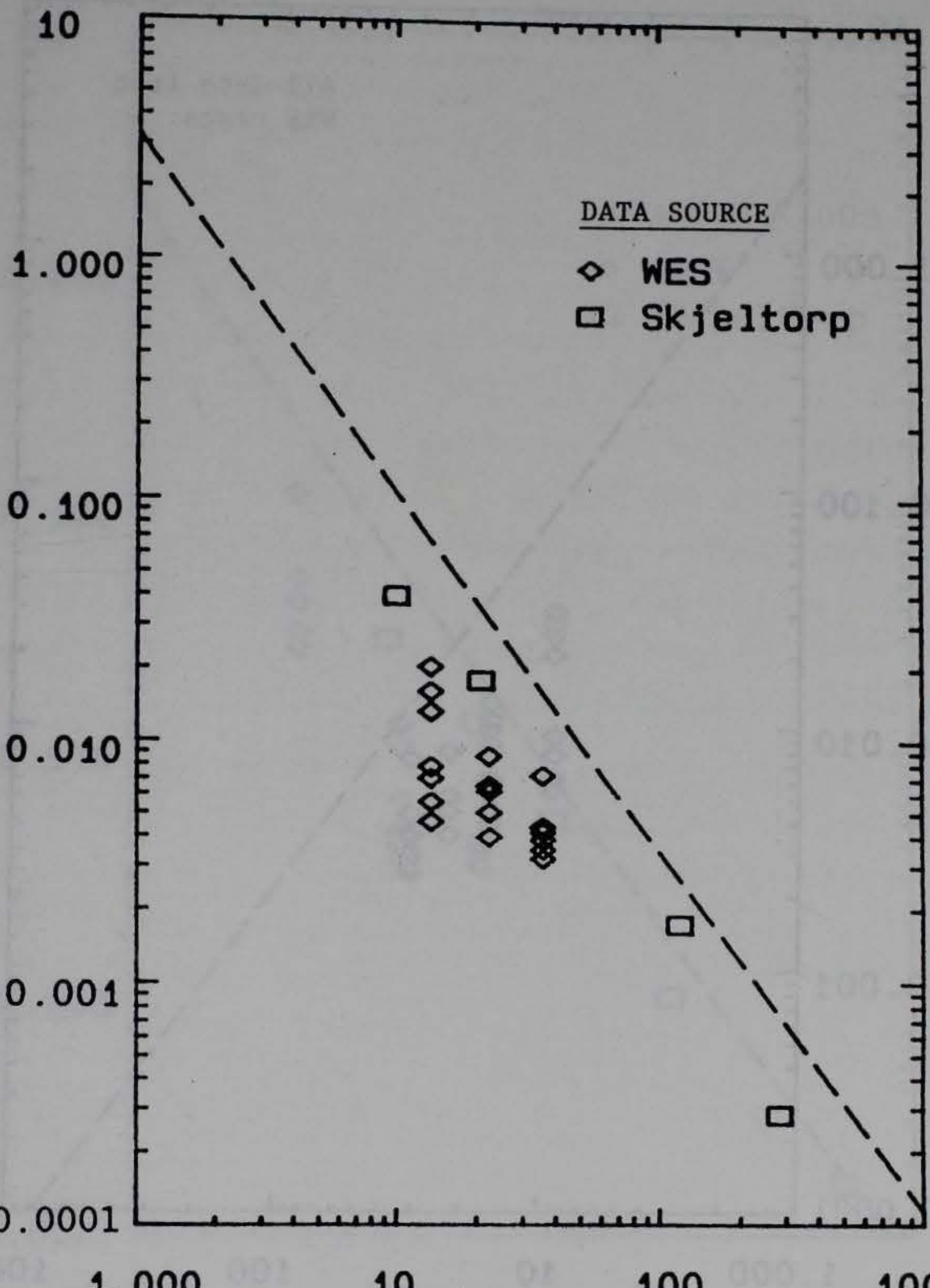


Figure 4.9. Normalized blast data (measured peak pressure "P" divided by chamber pressure "$P_e$") along a 30-degree line as a function of dimensionless distance (distance "R" divided by access tunnel diameter "D").

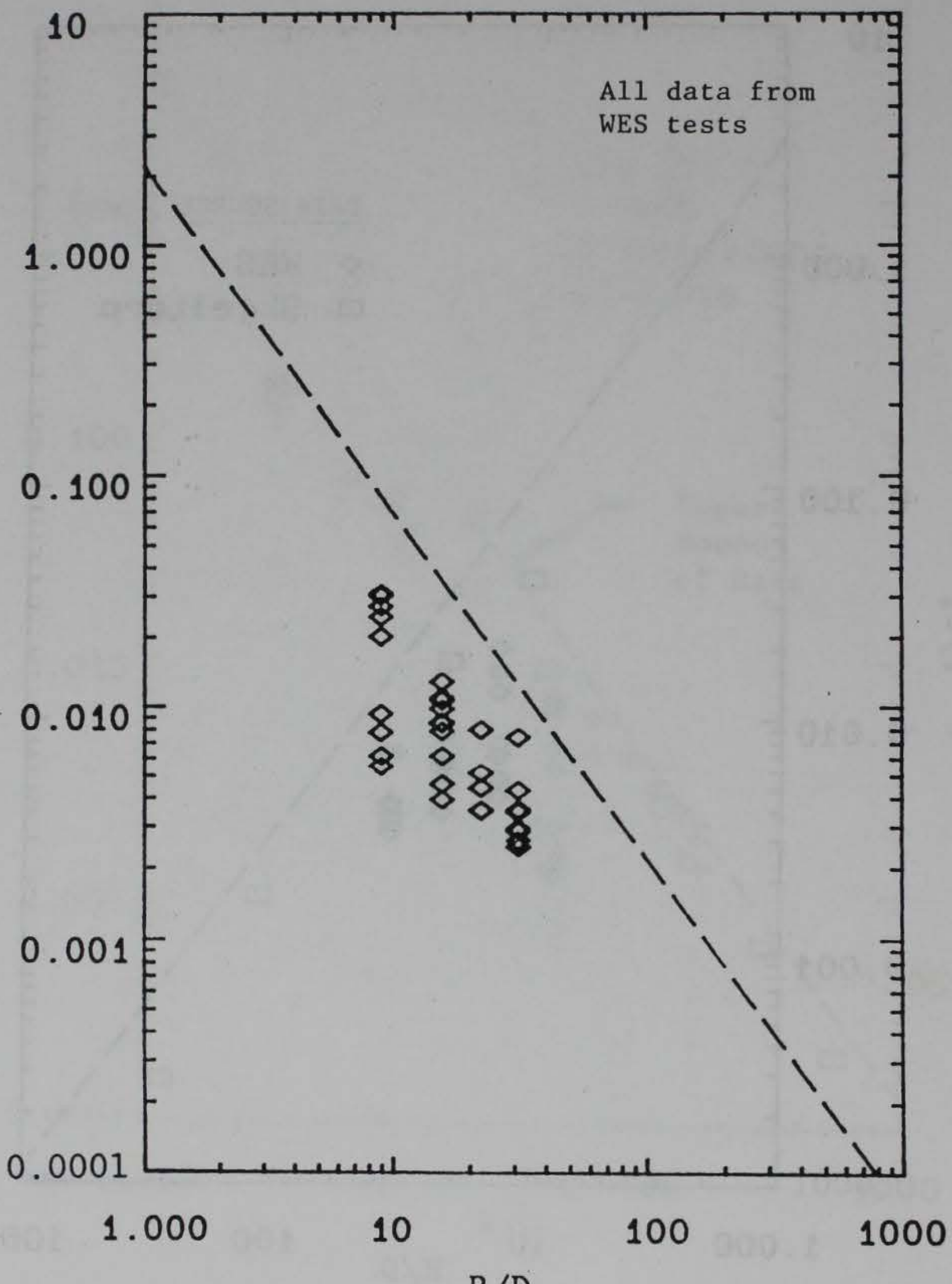


Figure 4.10. Normalized blast data (measured peak pressure "P" divided by chamber pressure "$P_e$") along a 45-degree line as a function of dimensionless distance (distance "R" divided by access tunnel diameter "D").

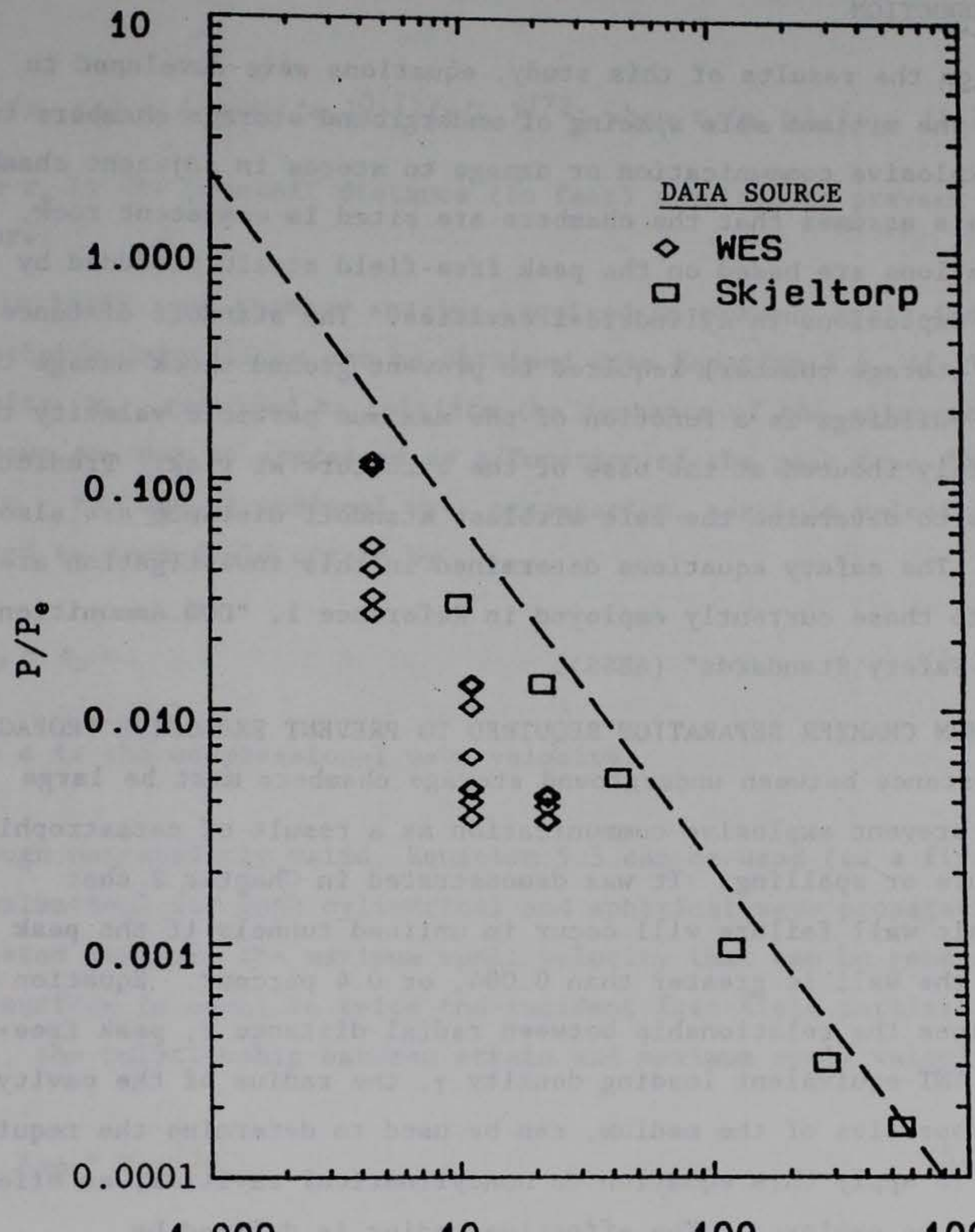


Figure 4.11. Normalized blast data (measured peak pressure "P" divided by chamber pressure "$P_e$") along a 60-degree line as a function of dimensionless distance (distance "R" divided by access tunnel diameter "D").

# CHAPTER 5

# PROPOSED EQUATIONS FOR SAFETY STANDARDS

## 5.1 INTRODUCTION

Based on the results of this study, equations were developed to determine the minimum safe spacing of underground storage chambers to prevent explosive communication or damage to stores in adjacent chambers. The analysis assumes that the chambers are sited in competent rock. These equations are based on the peak free-field strain produced by decoupled explosions in cylindrical cavities. The standoff distance (from the storage chamber) required to prevent ground shock damage to inhabited buildings is a function of the maximum particle velocity that may be safely induced at the base of the structure at risk. Predictive techniques to determine the safe airblast standoff distance are also reviewed. The safety equations determined in this investigation are compared to those currently employed in Reference 1, "DOD Ammunition and Explosive Safety Standards" (AESS).

## 5.2 MINIMUM CHAMBER SEPARATION REQUIRED TO PREVENT EXPLOSIVE PROPAGATION

The distance between underground storage chambers must be large enough to prevent explosive communication as a result of catastrophic wall failure or spalling. It was demonstrated in Chapter 2 that catastrophic wall failure will occur in unlined tunnels if the peak strain at the wall is greater than 0.004, or 0.4 percent. Equation 4.4, which defines the relationship between radial distance r, peak free-field strain $\epsilon$, TNT-equivalent loading density $\gamma$, the radius of the cavity a, and the properties of the medium, can be used to determine the required spacing. To apply this equation to noncylindrical cavities, an effective radius must be employed. The effective radius is defined by

$$a_e = (A/4\pi)^{1/2} \tag{5.1}$$

where $a_e$ is the effective radius in ft

and A is the cross-sectional area of the storage chamber in $ft^2$.

Substituting the strain threshold for catastrophic failure into Equation 4.4, we obtain

$$r_c/a_e = 2.39 \times 10^{12}(\gamma/E_o)^2; \text{ when } r_c/a_e < L/2a_e \qquad (5.2a)$$

and

$$r_c/a_e = 7.4 \times 10^2(L/a_e)^{0.75}(\gamma/E_o)^{1/2}; \text{ when } r_c/a_e > L/2a_e \qquad (5.2b)$$

where $r_c$ is the standoff distance (in feet) required to prevent tunnel closure.

Similarly, the chamber spacing required to prevent spall-induced, sympathetic detonations can be obtained from Equation 4.4, if the spall velocity, $v_{sp}$, required to initiate the contents of the adjacent chamber is known and can be expressed as a function of the peak free-field strain. For one-dimensional wave propagation, particle velocity $v_p$ is related to free-field strain by

$$v_p = \epsilon_p c \qquad (5.3)$$

where c is the compressional wave velocity.

Although not strictly valid, Equation 5.3 can be used (as a first approximation) for both cylindrical and spherical wave propagation. As indicated earlier, the maximum spall velocity that can be generated at a free surface is equal to twice the incident free-field particle velocity. Hence, the relationship between strain and maximum spall velocity is

$$\epsilon_{sp} = v_{sp}/2c \qquad (5.4)$$

where $v_{sp}$ is the upper bound of spall velocity at the wall.

Substituting for strain into Equation 4.4, the chamber separation ($r_{sp}$) required to prevent spall from initiating explosions in adjacent magazines is given by

$$r_{sp}/a_e = 1.53 \times 10^8(c\gamma/v_{sp}E_o)^2; \text{ when } r_{sp}/a_e < L/2a_e \qquad (5.5a)$$

$$r_{sp}/a_e = 66.2(L/a_e)^{0.75}(c\gamma/v_{sp}E_o)^{0.5}; \text{ when } r_{sp}/a_e > L/2a_e \quad (5.5b)$$

At low loading densities, the chamber spacing will be determined by 5.2a or 5.5a, which apply to the cylindrical decay region. As the loading density is increased, the required spacing will increase. Above some threshold loading density, the chamber spacing is determined by Equation 5.2b and 5.5b (which are based upon spherical decay). In this region, the standoff distance increases with an increase in loading density, chamber length, or chamber radius.

The chamber spacing required to prevent explosion communication is determined by the larger of the two values ($r_c$ or $r_{sp}$). However, it is not necessary to evaluate both $r_c$ and $r_{sp}$ to determine the required chamber spacing. If $\epsilon_p > 0.004$, catastrophic failure (Equation 5.2) dictates the spacing; conversely if $\epsilon_p < 0.004$, spalling (Equation 5.5) determines the chamber spacing.

In most cases, the minimum chamber spacing will be determined by catastrophic wall failure. This is because the spall velocity required to initiate explosives is typically on the order of 400 ft/sec, which corresponds to a strain at the wall that is well above the threshold strain (0.004) required for catastrophic failure. Spalling dominates only when sensitive explosives (initiated by very low spall velocities) are in the adjacent chamber. For example, for granite (assuming c equal to 15,000 ft/sec), spalling dominates only if the impact sensitivity of the contents is less than 120 ft/sec.

The equation used in the AESS (Reference 1) to determine the chamber separation distance ($r_{com}$) required to prevent explosive communication is

$$r_{com} = 1.5\ W^{1/3} \quad (5.6)$$

where W is the total explosive weight in the magazine (lbs).

It is difficult to make a general comparison between the equations developed above and Equation 5.6, because the latter does not explicitly address geometrical effects, spalling velocity, properties of the medium,

and nonlinear effects of decoupling. However, the equations can be compared by assuming some geometrical design, loading density, and spall velocity. For comparison purposes, the following values were assumed:

| | |
|---|---|
| Chamber length: | 262 ft |
| Chamber radius: | 12.24 ft |
| Spall velocity required for initiation of contents: | 400 ft/sec |
| Wave speed of rock: | 15,000 ft/sec |
| Young's Modulus: | $5 \times 10^6$ psi |

These dimensions are representative of a full-scale facility design. The distances required between the chambers, as predicted by the above equations, for spalling ($r_{sp}$), tunnel closure ($r_c$), and the current safety standards ($r_{com}$) are presented in Figure 5.1 for loading densities between 0.1 and 25 lb/ft$^3$.

The values shown in Figure 5.1 indicate that the current safety standards for chamber separation distance required to prevent explosive communication are very conservative. As indicated earlier, spalling should normally present no problem. In this example, a loading density of more than 11 lb/ft$^3$ is required to generate a spall velocity of 400 ft/sec at the tunnel wall. According to Equation 5.2, zero chamber separation is required to prevent tunnel closure if the loading density is below 3 lb/ft$^3$. This is because explosions in cavities with loading densities less than 3 lb/ft$^3$ produce strains at the cavity wall that are less than the incident strain (0.004) normally required to produce wall failure. Based on structural considerations alone, a chamber separation of one cavity diameter is recommended. Loading densities on the order of 2 to 3 lb/ft$^3$ are currently being considered. At these loading densities, standard construction procedures will preclude explosive communication in competent rock.

The above example demonstrates that current safety standards may significantly overestimate the chamber spacing required to prevent explosive communication. This occurs because the current standards

involve a lumped approach, and do not take into consideration geometrical effects, cylindrical geometry, decoupling, or the properties of the medium.

## 5.3 MINIMUM CHAMBER SEPARATION REQUIRED TO PREVENT DAMAGE TO STORES

An underground explosion will propagate a strain pulse through the surrounding rock, toward the wall of an adjacent (acceptor) storage chamber. Damage to the ammunition contents may occur if the strain at the acceptor chamber wall is sufficient to induce intermittent damage to the wall. Based upon experimental data obtained from several different media, intermittent boundary failures will not occur at peak strains less than 0.0003. Substituting for strain in Equation 4.4, the minimum spacing ($r_{cd}$) required between storage chambers to prevent damage to the contents is given by

$$r_{cd}/a_e = 2.39 \times 10^{14}(\gamma/E_o)^2 \quad ; \text{ when } r_{cd}/a_e < L/2a_e \tag{5.7a}$$

$$r_{cd}/a_e = 2.34 \times 10^{3}(L/a)^{0.75}(\gamma/E_o)^{1/2} \quad ; \text{ when } r_{cd}/a_e > L/2a_e \tag{5.7b}$$

According to the AESS, the chamber separation ($D_{cd}$) required to prevent damage to stored ammunition can be calculated by the following formulas:

$$D_{cd} = 3.5\ W^{1/3} \text{ (sandstone)} \tag{5.8a}$$

$$D_{cd} = 4.3\ W^{1/3} \text{ (limestone)} \tag{5.8b}$$

$$D_{cd} = 5.0\ W^{1/3} \text{ (granite)} \tag{5.8c}$$

where W is the weight of the explosive contents in lbs.

As in the previous case, a general comparison of Equations 5.7 and 5.8 is difficult; however, they were compared here using the geometrical design and medium properties used in the previous example. The chamber spacings required by AESS ($D_{cd}$) and by Equation 5.7 ($r_{cd}$) are presented in Figure 5.2 for loading densities from 0.1 to 25 lb/ft.

Theoretically, zero chamber separation is required for loading densities below 0.3 lb/ft. Explosions in storage chambers with low

loading densities result in wall strains below the incident peak strain typically required to damage unlined tunnels in rock. For the same reasons discussed in the preceding example, a minimum chamber separation of one cavity diameter is recommended.

For this particular geometrical configuration, the current safety standards are conservative. At loading densities of 2 and 3 $lb/ft^3$, Equation 5.7 suggests a chamber separation of 167 and 206 ft, respectively, as compared to the AESS requirement of 328 and 375 ft, respectively. The AESS standards are conservative for most magazine geometries. Equation 5.7 should more accurately predict the required chamber spacing.

## 5.4 INHABITED BUILDING STANDOFF DISTANCE

The required separation between the storage chamber and inhabited buildings can be determined from Equation 4.4 by employing the approximation given in Equation 5.3. Substituting for strain into Equation 4.4:

$$r_{ib}/a_e = 3.83 \times 10^7 (c\gamma/V_{ib}E_o)^2; \text{ when } r_{ib}/a_e \quad L/2a_e \qquad (5.9a)$$

and

$$r_{ib}/a_e = 46.8\ (L/a_e)^{0.75}(c\gamma/V_{ib}E_o)^{0.5}; \text{ when } r_{ib}/a_e \quad L/2a_e \qquad (5.9b)$$

where $r_{ib}$ is the standoff distance (ft) required for inhabited buildings, and $V_{ib}$ is the maximum ground motion velocity (ft/sec) which may be safely induced at the base of the structures.

Equation 5.9 defines the distance from the center of a storage chamber required for the particle velocities to decay to a specified value ($V_{ib}$), as a function of the loading density, dimensions of the cavity, and properties of the medium. The equations used in AESS do not address many of these parameters. According to AESS, the standoff distance required for inhabited buildings can be determined by:

$$D_{ib} = 2.33(\gamma/\gamma_t)^{0.3}\ W^{4/9} \text{ (sand, gravel, moist clay)} \qquad (5.10a)$$

$$D_{ib} = 11.8(\gamma/\gamma_t)^{0.3}\ W^{4/9} \text{ (soft rock)} \qquad (5.10b)$$

$$D_{ib} = 13.3(\gamma/\gamma_t)^{0.3}\ W^{4/9} \text{ (hard rock)} \qquad (5.10c)$$

where $D_{ib}$ is the standoff distance (ft)

$W$ is the total TNT-equivalent charge weight (lbs)

$\gamma$ is the loading density (lb/ft$^3$)

$\gamma_t$ is the density of TNT (lb/ft$^3$)

These equations are predicated upon maximum allowable particle velocities of 2.4, 4.5 and 9 in./sec, respectively, at the base of structures in these geologies.

The AESS equations have several disadvantages. They are apparently based upon the decoupling effects of spherical cavities and consequently do not take into consideration the additional decoupling effects of cylindrical cavities of finite length. The predictive technique also does not offer the capability to calculate the standoff distance required for structures that might be damaged at significantly higher or lower particle velocities than those assumed.

As in the previous case, the current standards can be most effectively compared to the results of this investigation by considering a specific example. The dimensions and rock properties used in the previous comparison will be assumed. To be consistent with Equation 5.10, a particle velocity of 9 in./sec was assumed in Equation 5.9. The standoff distance required according to Equation 5.10c is shown in Figure 5.3 for loading densities between 0.1 and 25 lb/ft$^3$. The chamber separation required by the AESS equation is consistently larger than that required by Equation 5.9. For this particular example, the AESS standards are increasingly conservative with loading density. The AESS equation appears to have a safety factor of at least 1.29 at a loading density of 0.2 lb/ft$^3$, and a safety factor of 4.11 at 25 lb/ft$^3$. For loading densities of 2 to 3 lb/ft$^3$, the AESS equation requires standoff distances approximately twice those of Equation 5.9.

## 5.5 AIRBLAST STANDOFF DISTANCE

To determine the airblast standoff distance, it is necessary to predict accurately the pressure at the tunnel portal, and the rate of pressure decay with distance in various directions beyond the portal.

Predictive techniques have been developed to determine the pressure generated at the portal for elementary geometries if the loading densities are between 1 and 25 $lb/ft^3$. Typical equations were given in Chapter 1. An empirical dimensionless equation which delineates the decay of the peak free-field pressure as a function of the portal exit pressure, the effective diameter of the tunnel, and distance was developed in Chapter 4:

$$P/P_E = C_1(r/D_e)^{-1.5} \qquad (5.11)$$

where P is the peak free-field overpressure (psi)

$P_E$ is the exit pressure at the tunnel portal (psi)

D is the effective diameter of the tunnel (ft)

and $C_1$ is a constant functionally dependent upon direction.

Based upon the results obtained by Gurke and Scheklinski (Reference 15), Jenssen (Reference 35), and this investigation, Equation 5.11 will predict accurate standoff distances near and along the extended centerline for loading densities between 1 and 2.5 $lb/ft^3$, for exit slopes between 0 and 30 degrees. At lower loading densities, the predicted standoff distances will be increasingly conservative. Prudent use of Equation 5.11 is required.

Equation 5.11 is based upon an access tunnel which exits parallel and tangent to smooth terrain. The local topography can significantly alter the standoff distance required. In general, the attenuating effects of vegetation and the natural surface roughness tend to make the estimates conservative. Falling terrain slopes (with respect to the extended centerline of the tunnel) tend to decrease the pressure levels. Conversely, rising slopes may tend to increase the required standoff distance. Careful consideration should be given to any surface characteristics (hillsides, valleys, buildings, etc.) which could focus the shock wave.

Equation 5.11 may not be valid for large loading densities. As indicated in Figure 2.1, at TNT loading densities greater than 0.07 $lb/ft^3$, oxygen-deficient combustion products result. Secondary chemical reactions may occur in the access tunnel and/or at the portal.

A secondary explosion at the portal would increase the free-field blast pressure and could alter the directional characteristics of the peak overpressure. The magnitude and location of a secondary explosion would depend upon the chemical composition and the total mass of explosive.

Large loading densities may not necessarily result in large blast pressures at the portal. Partial or complete ground shock closure of the tunnel exiting the storage chamber may occur. In this investigation, a loading density of 25.3 $lb/ft^3$ produced partial closure and reduced the peak free-field blast by approximately 70 percent. Tunnel closure has occurred on several full-scale tests, and is sometimes deliberately planned to prevent venting. As a result, for loading densities above 2.5 $lb/ft^3$, Equations 2.1 and 5.11 should be used with caution and should not be employed for large loading densities.

Existing equations cannot be used to determine the pressure generated at the portal of complex geometries, because these equations are empirical relationships which define the peak pressure based upon total volume of the complex and the total charge weight. As a result, they do not explicitly address the problem of shock propagation through complex geometries. If the blast pressure generated at the portal is determined experimentally for a complex underground geometry, Equation 5.11 may be used to predict the required standoff distance if the loading density is not sufficiently large to produce secondary explosions outside the portal.

The airblast standoff distance (D) is determined in the AESS by equations of the following form:

$$D_\theta = C_\theta \, W^{1/3} \tag{5.12}$$

where $D_\theta$ is the required standoff distance along a line which is at a horizontal angle of $\theta$ degrees from the extended centerline

and W is the net explosive weight (lbs)

$C_\theta$ is a constant functionally dependent upon the direction from the portal.

This equation may not provide reliable estimates of the required standoff distance in all cases, because it applies only to short, straight tunnels leading directly from a chamber, and does not assess the geometrical effects on shock propagation through an underground complex.

In summary, accurate airblast standoff distance can be determined for elementary tunnel/chamber geometries at loading densities between 1 and 2.5 $lb/ft^3$. At high loading densities, the current AESS equations predict substantially larger standoff distances than required. For complex geometries, the airblast standoff distance can be determined only if experimental data for that geometry is available to predict a portal exit pressure. For loading densities large enough to produce secondary explosions inside the tunnel complex or at the portal, no predictive techniques are currently available.

## 5.6 SUMMARY

Equations have been developed in this study to predict various safety standoff distances required as a result of explosions in underground magazines. The equations for ground shock address magazine geometrical effects, explosion decoupling, and the properties of the rock medium. Additionally, the chamber separation distance required to prevent symathetic detonations in adjacent chambers by rock spalling is functionally dependent on the impact sensitivity of the contents.

The standoff distance required to prevent ground shock damage to inhabited buildings is related to the peak ground shock threshold velocity of incipient damage to the structure. The equations developed in this study should yield conservative standoff distances for two reasons. First, they are based on upper bound strain measurements. In almost all instances, the actual strain field will be less than the assumed upper bound. Second, the strain data was obtained around a chamber in which the contents were detonated essentially instantaneously. In full-scale magazines, sequential detonation of the contents over some finite time period is much more probable.

The current AESS equations do not address chamber geometry or decoupling effects, nor do they have a capability to address variations in media properties. Essentially, they are lumped equations which, in

general, will predict very conservative standoff distances, which can result in increased construction costs or real estate requirements (for buffer zones).

The data obtained in this study corroborate equations proposed by Skjeltorp (Reference 4) to determine the standoff distance required to prevent damage to inhabited buildings by airblast. However, these equations are valid only if the loading density is sufficiently small that secondary explosions do not occur near or outside the portal.

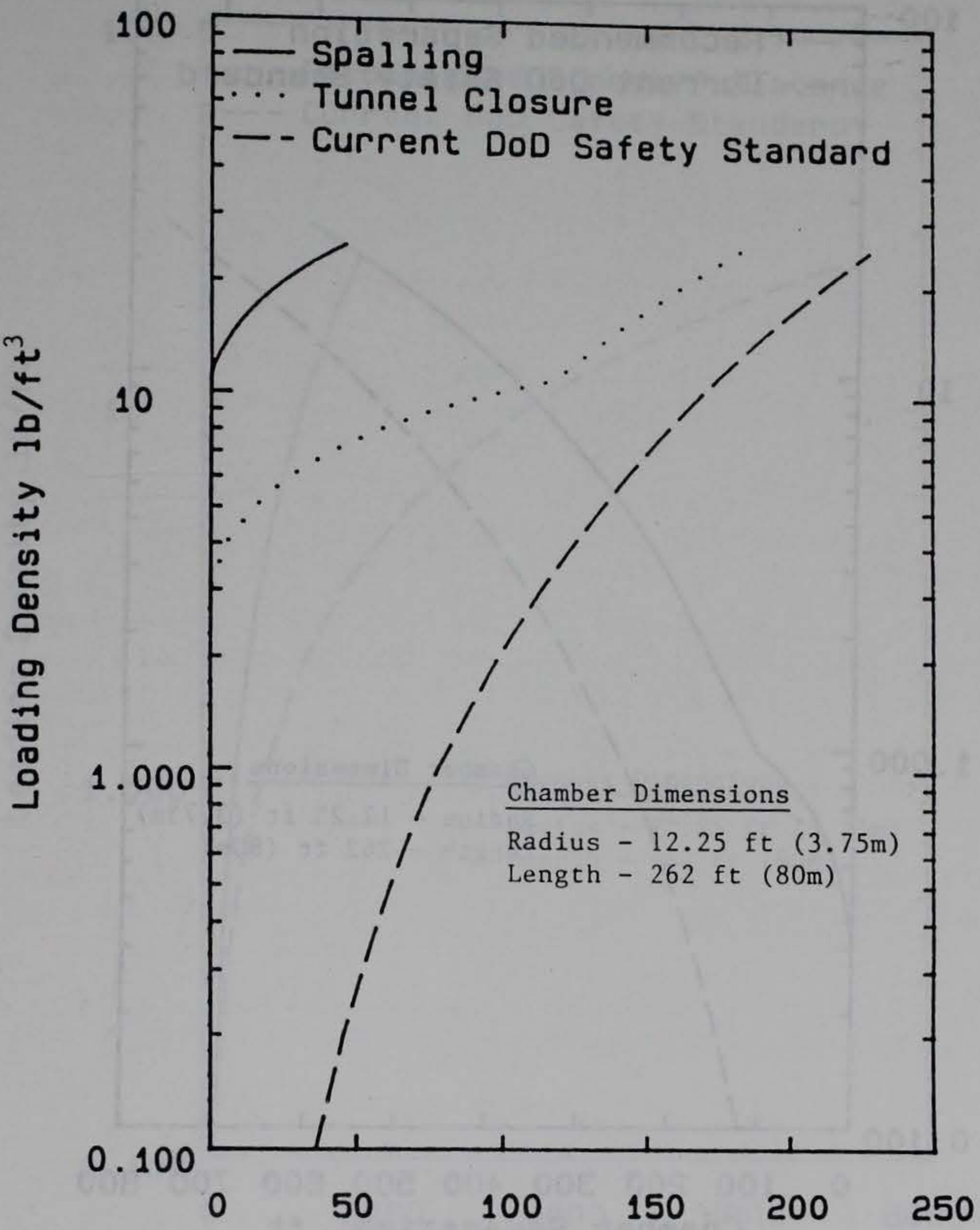


Figure 5.1. Calculated storage chamber separation required to prevent tunnel closure and explosive communication (by spall), compared to the current DOD Safety Standard (for a typical design in granite).

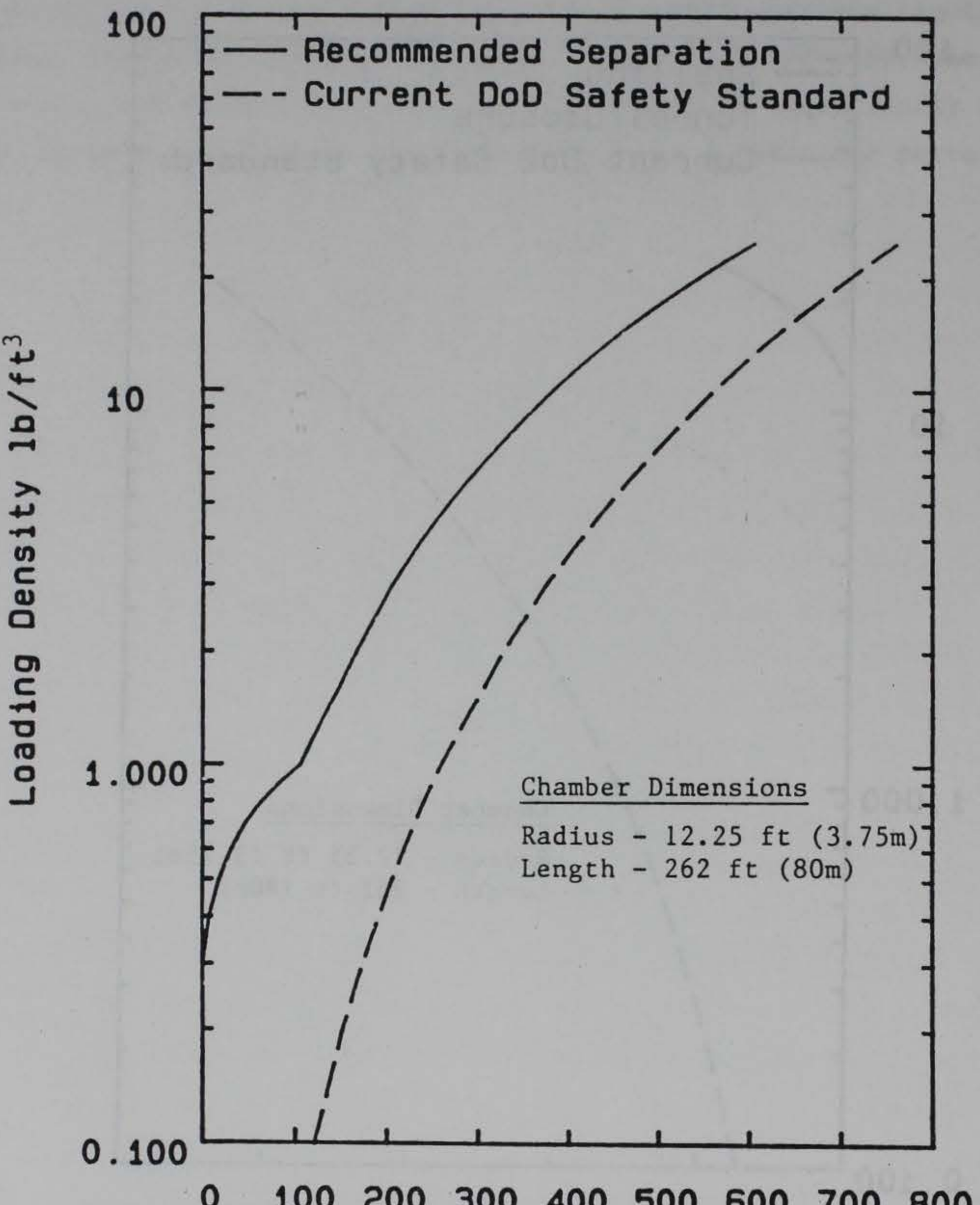


Figure 5.2. Calculated storage chamber separation required to prevent damage to contents, compared to current DOD Safety Standards (for a typical design in granite).

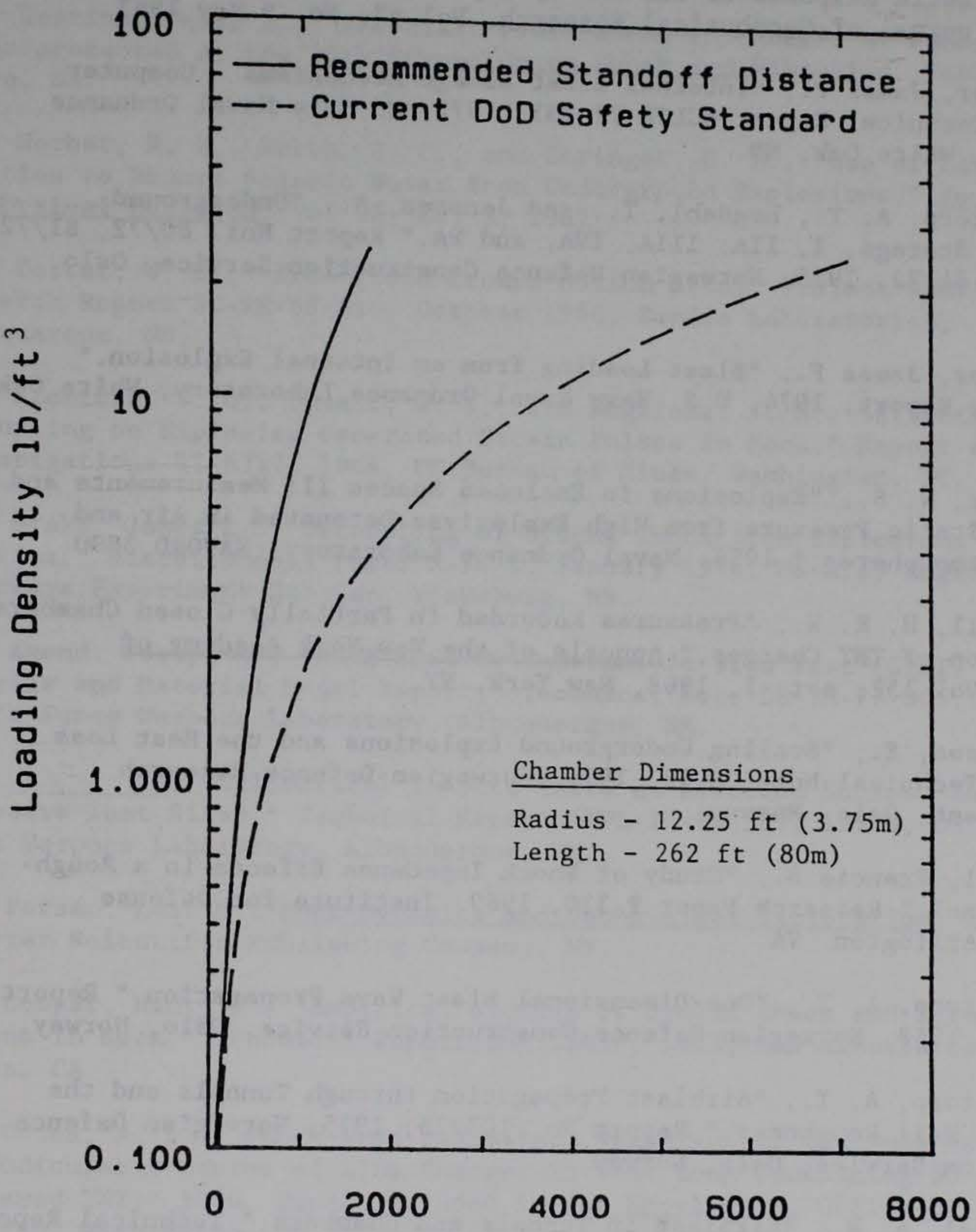


Figure 5.3. Calculated standoff distance required to prevent damage to inhabited buildings, compared to current DOD Safety Standards (for a typical design in granite).

## REFERENCES


1. "DOD Ammunition and Explosive Safety Standards," Report No. DOD 5154.4S, Washington, DC.

2. Brode, H. L., and Parkin, B. R., "Calculations of the Blast and Close-In Elastic Response of the Cavity Explosions in the Cowboy Program," Journal of Geophysical Research, Vol 68, No. 9 May 1963.

3. Proctor, James F., "Internal Blast Damage Mechanisms - Computer Program," Technical Report NCLTR 72-231, 1972, US Navy Naval Ordnance Laboratory, White Oak, MD.

4. Skjeltorp, A. T., Hegdahl, T., and Jenssen, A., "Underground Ammunition Storage, I, IIA, IIIA, IVA, and VA," Report Nos. 80/72, 81/72, 83/72, and 84/72, 1975, Norwegian Defence Construction Service, Oslo, Norway.

5. Proctor, James F., "Blast Loading from an Internal Explosion," Preliminary Report, 1974, U.S. Navy Naval Ordnance Laboratory, White Oak, MD.

6. Filler, W. S., "Explosions in Enclosed Spaces II: Measurements and Theory on Static Pressure from High Explosives Detonated in Air and Nitrogen Atmospheres," 1956, Naval Ordnance Laboratory, NAVORD 3890.

7. Weibull, H. R. W., "Pressures Recorded in Partially Closed Chambers at Explosion of TNT Charges," Annuals of the New York Academy of Sciences, Vol 152, Art. 1, 1968, New York, NY.

8. Stromsoe, E., "Scaling Underground Explosions and the Heat Loss Problem," Technical Note UM-15, 1971, Norwegian Defence Research Establishment, Oslo, Norway.

9. Porzel, Francis B., "Study of Shock Impedance Effects in a Rough-Walled Tunnel," Research Paper P-330, 1969, Institute for Defense Analyses, Arlington, VA.

10. Skjeltorp, A. T., "One-Dimensional Blast Wave Propagation," Report No. 48/69, 1968, Norwegian Defence Construction Service, Oslo, Norway.

11. Skjeltorp, A. T., "Airblast Propagation through Tunnels and the Effects of Wall Roughness," Report No. 103/75, 1975, Norwegian Defence Construction Service, Oslo, Norway.

12. Kriebel, A. R., "Airblast in Tunnels and Chambers," Technical Report URS 7050-2, 1972, URS Research Company, San Mateo, CA.

13. Schmidt, K. G., "Investigations of Underground Explosions with Model Tests," Technical Note UM-238, 1976, Norwegian Defence Research Establishment, Kjeller, Norway.

14. Fredricksen, G., and Jenssen, A., "Underground Ammunition Storages," Report No. 59/70, 1970, Norwegian Defence Construction Service, Oslo, Norway.

15. Gurke, G., and Scheklinski, G., "Underground Ammunitions Storage Model Tests," Report E 12/77, 1977, Ernst-Mach Institut, Freiburg, Germany.

16. Westine, Peter S., "The Blast Field about the Muzzle of Guns," 1969, paper presented at the 39th Symposium on Shock and Vibration, Pacific Grove, CA.

17. Herbst, R. F., Werth, G. C., and Springer, D. L., "Use of Large Cavities to Reduce Seismic Waves from Underground Explosions," Journal of Geophysical Research, Vol 66, No. 3, 1961.

18. Perret, W. R., "Free-Field Ground Motion Study, Project Sterling," Research Report SC-RR-68-410, October 1968, Sandia Laboratories, Albuquerque, NM.

19. Atchison, T. C., Duvall, W. I., and Pugliese, J. M., "Effects of Decoupling on Explosion-Generated Strain Pulses in Rock," Report of Investigations RI-6333, 1964, US Bureau of Mines, Washington, DC.

20. Drake, James L., "Decoupling of Ground Shock from Explosions in Rock Cavities," Miscellaneous Paper N-74-1, January 1974, US Army Engineer Waterways Experiment Station, Vicksburg, MS.

21. Amend, Joseph H., "HAVE HOST Cylindrical In Situ Test (CIST) Data Analysis and Material Model Report," Technical Note DE-TN-77-005, 1977a, US Air Force Weapons Laboratory, Albuquerque, NM.

22. _____, "Cylindrical In-Situ Tests at Selected Nuclear and High-Explosive Test Sites," Technical Report AFWL-TR-76-209, 1977b, US Air Force Weapons Laboratory, Albuquerque, NM.

23. Persen, Leif N., Rock Dynamics and Geophysical Exploration, 1975, Elsevier Scientific Publishing Company, NY.

24. Cooper, Henry F., "Empirical Studies of Ground Shock and Strong Motions in Rock," Technical Report DNA 3245F, 1973, R&D Associates, Santa Monica, CA.

25. Coles, J. S., "Shock-Wave Parameters Measured off the Ends and Perpendicular Bisector of Line Charges 25 Feet Long Containing 50 Pounds of Flexed TNT," 1950, Paper included in The Shock Wave, Office of Naval Research, Washington, DC.

26. Baker, Wilfred E., Explosions in Air, 1973, University of Texas Press, Austin, TX.

27. Department of the Army; "Employment of Atomic Demolition Munitions (ADM)", Field Manual FM 5-26, December 1965, Washington, DC.

28. Engineering Research Associates, et al., "Underground Explosion Test Program, Technical Report 4, Granite and Limestone, Volume I," August 1952, St. Paul, Minnesota.

29. Engineering Research Associates, et al., "Underground Explosion Test Program, Technical Report 5, Sandstone, Volume I," February 1953, St. Paul, Minnesota.

30. Joachim, Charles E., "ESSEX - DIAMOND ORE Research Program--Tunnel Destruction: A State-of-the-Art Summary," Miscellaneous Paper N-78-1, January 1978, US Army Engineer Waterways Experiment Station, Vicksburg, MS.

31. Hendron, A. J., Jr., Clark, G. B., and Strange, J. N., "Damage to Model Tunnels Resulting from an Explosively-Produced Impulse; Report 1, Test in a Simulated Rock Mass of Medium Strength," Research Report 1-6, May 1965, US Army Engineer Waterways Experiment Station, Vicksburg, MS.

32. Swift, R. P., "Examination of the Mechanical Properties of a Kayenta Sandstone from the Mixed Company Site," DNA 3683F, July 1975, Physics International Company, San Leandro, CA.

33. Rinehart, John S., Stress Transients in Solids, 1975, Hyperdynamics, Santa Fe, NM.

34. Gottlieb, J. J., "Investigation of the Pressure after an Explosion in a Closed Vessel," DRES Suffield Technical Paper No. 371, 1971, Defense Research Establishment/Suffield, Suffield, Canada.

35. Jenssen, A., "Underground Ammunition Storages Chamber Pressure," Informal Working Paper for NATO Group of Experts AC/258, Underground Storage Sub-Group, preliminary draft yet to be published, Norwegian Defence Construction Service, Oslo, Norway.

36. Culbertson, D. W., "An Investigation of the Recoil Forces Produced by Detonation of High Explosive charges in the 16"/45 Cal Gun Mk 6 Mod 1," Technical Memorandum T-3/62, November 1962, US Naval Weapons Laboratory, Dahlgren, VA.

37. Cook, M. A., The Science of High Explosives, 1958, Reinhold Publishing Corp., New York, NY.

38. James, D. J. and Rowe, R. D., "Measurement of Steady Overpressure Loading on the Wall of a Spherical Cavity Resulting from the Detonation of a Single HE Charge at the Center," ARE No. E3/64, 1964, Atomic Weapons Research Establishment, Foulness, England.

# BIBLIOGRAPHY

Murphy, B. F., "Particle Motions Near Explosion in Halite," Journal of Geophysical Research, Vol 66, No. 3, March 1961.

Nicholls, H. R., Hooker, V., and Duvall, W. I., "Project Cowboy, Dynamic Rock Mechanics Investigations," APRL Report No. 38-3.2, September 1960, U.S. Bureau of Mines, Applied Physics Research Laboratory, College Park, MD.

Swift, L. M. and Wells, W. M., "Close-In Earth Motions, Project HOBO," Report No. UCRL 6397, March 1961, Stanford Research Institute, Menlo Park, Ca.